Journal of Advanced Research xxx (xxxx) xxx

Contents lists available at ScienceDirect

Journal of Advanced Research

journal homepage: www.elsevier.com/locate/jare

Development of novel broad-spectrum amphipathic antimicrobial peptides against multidrug-resistant bacteria through a rational combination strategy

Jing Zhang [a,b,1], Liang Luan [c,1], Youdong Xu [d], Shuyuan Jiang [a,b], Wenpeng Zhang [a], Long Tian [a], Weifeng Ye [e], Jiaqi Han [a], Changhao Zhang [b,*], Taoran Wang [a,*], Qingbing Meng [a,*]

[a] State Key Laboratory of National Security Specially Needed Medicines, Beijing Institute of Pharmacology and Toxicology, Beijing 100850, China
[b] Key laboratory of Natural Medicines of the Changbai Mountain, Ministry of Education, College of Pharmacy, Yanbian University, Yanji 133002, China
[c] Department of Laboratory Medical Center, General Hospital of Northern Theater Command, No.83, Wenhua Road, Shenhe District, Shenyang 110016, China
[d] National Center for Protein Sciences (Beijing), Beijing Institute of Lifeomics, State Key Laboratory of Proteomics, Beijing Proteome Research Center, Beijing 102206, China
[e] Center of Clinical Laboratory, Beijing Friendship Hospital, Capital Medical University, Beijing 100050, China

HIGHLIGHTS

- A series of $sC18_{4b}$ -derived cationic amphipathic antimicrobial peptides were designed by a combination strategy.
- P-α-02-B, a screened analogue, displayed broad-spectrum and potent antimicrobial activity with high bacterial selectivity
- P-α-02-B exhibited superior plasma stability, overcoming a major limitation of traditional AMPs.
- When combined with levofloxacin, P-α-02-B showed a synergistic antimicrobial effect
- In vivo studies confirmed the favorable therapeutic efficacy of P-α-02-B, both as a standalone agent and in combination therapy, against multidrug-resistant bacterial infections.

GRAPHICAL ABSTRACT

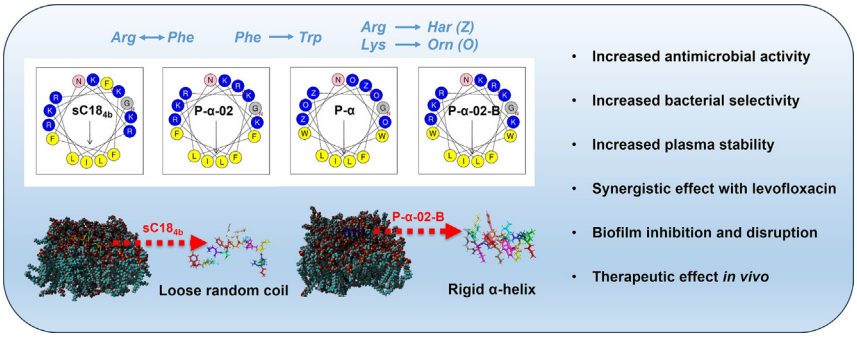

ARTICLE INFO

Article history:
Received 6 November 2024
Revised 27 December 2024
Accepted 16 January 2025
Available online xxxx

Keywords:
Antimicrobial Peptides
Cationic

ABSTRACT

Introduction: In recent years, cationic amphipathic antimicrobial peptides (AMPs) have shown great promise in combating antibiotic resistance on account of their distinctive membrane-disruptive mechanism. However, the clinical application of AMPs is restricted by their unsatisfactory stability and safety. Although attempts have been made to improve the stability and safety of AMPs, many of them are accompanied by a decline in their antimicrobial activity and bacterial selectivity.
Objectives: To develop AMPs with excellent and balanced antimicrobial activity, stability, and safety using a combination strategy.
Methods: A series of $sC18_{4b}$-derived peptide analogues were designed by a combination strategy of subtly adjusting the charges, hydrophobic properties, and introducing specific unnatural amino acids in a

* Corresponding authors.
E-mail addresses: zhangch@ybu.edu.cn (C. Zhang), wtr1372957199@126.com (T. Wang), nankaimqb@sina.com (Q. Meng).
[1] These authors contributed to work equally.

https://doi.org/10.1016/j.jare.2025.01.029
2090-1232/

Please cite this article as: J. Zhang, L. Luan, Y. Xu et al., Development of novel broad-spectrum amphipathic antimicrobial peptides against multidrug-resistant bacteria through a rational combination strategy, Journal of Advanced Research, https://doi.org/10.1016/j.jare.2025.01.029

Amphipathic
Combination strategy
Multidrug-resistant bacteria

well-balanced manner. The antimicrobial activity, cytotoxicity, hemolytic activity, stability, anti-biofilm activity, mechanism of action, synergistic effects, *in vivo* efficacy, and pharmacokinetics of the analogues were evaluated.

Results: Among these analogues, P-α-02-B stood out for its broad-spectrum and potent antimicrobial activity, anti-biofilm activity, desirable bacterial selectivity, high plasma stability, and synergistic effect with antibiotic levofloxacin. P-α-02-B exhibited strong membrane disturbance effect, which could be explained by its rigid α-helical structure revealed by molecular dynamics simulations. More importantly, P-α-02-B showed favorable therapeutic efficacy *in vivo*, whether used alone or in combination with levofloxacin.

Conclusion: P-α-02-B is a promising antimicrobial agent for MDR bacterial infections, demonstrating the effectiveness of the combination strategy for AMP development.

Introduction

The rapid spread of infectious diseases resulting from multidrug-resistant (MDR) bacteria, which are difficult for conventional antibiotics to cope with, poses a great threat to our health system [1–3]. There is an urgent need for novel and efficacious antimicrobial drugs. In recent years, AMPs with broad-spectrum and potent antimicrobial activity against MDR bacteria has raised great concern and become promising alternatives to conventional antibiotics [4]. AMPs are generated by numerous life forms and function as crucial elements of the host defense system [5]. For the majority of AMPs, their principal mechanism of action lies in disrupting the bacterial membrane, a process that is both swift and non-specific [6]. Due to the highly-conservative structures of bacterial membranes, it is difficult for AMPs to induce drug-resistance among MDR bacteria [7–9]. Besides, certain AMPs demonstrate synergistic effects when combined with conventional antibiotics because of their complementary action mechanisms [10,11], and many AMPs could inhibit and disrupt bacterial biofilms, which are tolerant to conventional antibiotics [12,13].

Although AMPs possess the advantages above stated, their clinical application is hampered by their susceptibility to degradation, which results from the inherent characteristics of peptide drugs [8]. Besides, the non-specific cytotoxicity of AMPs brings about certain safety risks in clinical practice [5]. For example, the commercial AMPs, gramicidin and polymyxins, have been reported to cause adverse events like nephrotoxicity and neurotoxicity [14]. Several strategies such as cyclization, truncation, and terminal modification have been adopted to overcome the drawbacks of AMPs. However, most of the time, these strategies fail to achieve an equilibrium between the antimicrobial activity, stability and safety of AMPs [15]. Developing novel AMPs with effective antimicrobial potency, high resistance to proteolysis, and low toxicity for clinical application remains a challenging issue.

For cationic amphipathic AMPs, moderate amounts of cationic and hydrophobic moieties can facilitate their binding to and inserting into bacterial membranes, which is indispensable for the membrane disruption action [7,16,17]. Regulating the positive charges and hydrophobic properties (hydrophobicity and hydrophobic moment) are proven to be effective in improving the antimicrobial activity and selectivity index (SI) of AMPs [18]. Besides, mounting evidence suggests that the basic amino acids in cationic AMPs, known as Lys and Arg, are susceptible to plasma digestion, which results in a short half-life as well as the loss of antimicrobial activity of AMPs [19]. Several approaches have been utilized to prolong the half-life of cationic AMPs, among which the incorporation of unnatural amino acids not only protects AMPs from the proteolysis by plasma, but also increase their SI [20–22] .

To develop AMPs with excellent and well-balanced antimicrobial activity, stability and safety, a combination strategy of subtly adjusting the charges, hydrophobic properties, and introducing specific unnatural amino acids was employed. In this study, a sequence of $sC18_{4b}$-derived peptide analogues were designed and synthesized. The antimicrobial activity of the peptides against both standard and MDR bacteria was evaluated, and their cytotoxicity, hemolytic activity and stability were investigated. P-α-02-B, which was screened to be the preferred compound, was further investigated on its anti-biofilm potentials, mode of actions, synergistic effects with levofloxacin, *in vivo* antimicrobial activity and pharmacokinetic in detail.

Materials and methods

Materials

Rink amide resin was obtained from Nankai Hecheng (Tianjin, China). Fmoc-protected amino acids were obtained from GL Biochem (Shanghai, China). N,N'-Diisopropylcarbodiimide (DIC), trifluoroacetic acid (TFA), m-cresol, anisole, ethanedithiol, trifluoroethanol (TFE) were obtained from J & K Scientific (Beijing, China). Ethyl 2-cyano-2-(hydroxyimino) acetate (Oxyma) was obtained from CSBio (Shanghai, China). Piperidine and acetic anhydride were obtained from Sinopharm Chemical Reagent Co., Ltd (Shanghai, China). Dulbecco's Modified Eagle Medium (DMEM), penicillin–streptomycin (PS), fetal bovine serum (FBS), 0.25 % trypsin-EDTA and phosphate-buffered saline (PBS) were obtained from Gibco (Grand Island, NY, USA). Nutrient broth and nutrient agar were purchased from Beijing Land Bridge Technology Co., Ltd (Beijing, China). The Cell Counting Kit-8 (CCK-8) was obtained from Dojindo Molecular Technologies, Inc (Kumamoto, Japan). Levofloxacin and meropenem trihydrate were obtained from Macklin (Shanghai, China). Crystal violet, 4-(2-hydroxyethyl)-1-pi perazineethanesulfonic acid (HEPES), 1-*N*-phenylnaphthylamine (NPN) and 2-Nitrophenyl β-D-galactopyranoside (ONPG) were obtained from Aladdin (Shanghai, China). Triton X-100, Propidium iodide (PI), 6-diamidino-2-phenylindole (DAPI) were purchased from Beijing Solarbio Science & Technology Co., Ltd (Beijing, China).

Peptide synthesis and purification

Peptides with amidated C-terminus were synthesized by a microwave peptide synthesizer (CEM, USA). Briefly, the Fmoc-protected amino acids were attached to the rink amide resin sequentially. Piperidine/DMF (20 %, *v*/*v*) solution was employed as the deprotection agent and DIC/Oxyma as the coupling reagent. Acetic anhydride was coupled to the N-terminus of the peptides. The final cleavage was carried out at 0 °C (0.5 h) and then at room temperature (2.5 h) successively, using a cleavage reagent (TFA (90 %)/anisole (5 %)/m-cresol (3 %)/ethanedithiol (2 %)).

Circular dichroism (CD) measurements

Peptides were dissolved in the TFE/PBS (50 %, *v*/*v*) solution, which was capable of mimicking the membrane environment. The parameters of the CD instrument (Claix, France) were set as follows: wavelength between 185 and 270 nm, a time response of 2 s, a resolution of 0.5 nm, a bandwidth of 4.0 nm, and a speed of 50 nm/min. After background subtraction and smoothing, the final curves of the peptides were obtained.

Bacterial strains

The MDR bacterial strains, including *S. aureus*, *E. aerogenes, A. baumannii, C. freundii* were obtained from the Department of Laboratory Medical Center of General Hospital of Northern Theater Command (Shenhe District). The standard bacterial strains, including *E. coli* ATCC 25922 and *B. subtilis* ATCC 6633 were obtained from China National Institute for the Control of Pharmaceutical and Biological Products (Beijing, China). All bacterial strains were stored in 50 % sterile glycerol at −80 °C.

Minimal inhibitory concentrations (MICs) assay

The MIC assay was performed according to the broth microdilution procedure. Briefly, 50 μL of sterile broth was added into each well of plates. Then, samples dissolved in physiological saline (50 μL) were added to the first lines of plates, and then two-fold serial dilutions were carried out. Each sample was repeated in triplicate. Subsequently, bacterial suspensions (50 μL; 1.0×10^6 CFU/mL) were added into each well. After an incubation at 37 °C for 16 h while being constantly agitated, the MIC was ascertained by visual observation in combination with the absorbance measurement at 600 nm with a SpectraMax M5 microplate reader (Molecular, USA).

Hemolytic assay

The hemolytic assay was performed by subjecting human erythrocytes to peptide samples and gauging the amount of released hemoglobin. Fresh human red blood cells (hRBCs) were obtained from the heparinized human blood offered by the Clinical Laboratory Center of Beijing Friendship Hospital. After centrifugation (1800 rpm, 4 °C, 5 min) and PBS washing three times, the concentrated hRBCs were resuspended in PBS to prepare a 5 % (*v*/*v*) erythrocyte suspension. 10 μL of PBS was added into each well of plates. Then, samples dissolved in PBS (10 μL) were added to the first lines of plates, followed by two-fold serial dilutions. Each sample was repeated in quintic. Next, 90 μL of the suspension was added into each well, leading to a final peptide concentration ranging from 0.78 μM to 50 μM. PBS and 1 % Triton X-100 served as negative and positive controls, respectively. The plates were kept at 37 °C for 1 h and then centrifuged at 3000 rpm for 5 min. The supernatant absorbance at 405 nm was measured by a SpectraMax M5 microplate reader (Molecular, USA) to obtain the hemolysis data. Median hemolytic concentration (HC_{50}) was obtained with the help of SPSS software. SI was calculated as follows:

$$SI = HC_{50}\ (\mu M) \,/\, \text{geometric mean (GM) of MICs}\ (\mu M).$$

Cytotoxicity assay

The cytotoxicity of peptides was evaluated by CCK-8 assay with the human embryonic kidney 293 T cell line. After incubation for 24 h, the 293 T cells in 96-well plates were subjected to different concentrations of peptides dissolved in DMEM medium (100 μL) and incubated for 24 h. Later, the solution of each well was mixed with CCK-8 reagent (10 μL). Each sample was repeated in quintic. After incubation for 2 h at 37 °C, the absorbance at 450 nm was measured using a SpectraMax M5 microplate reader (Molecular, USA).

Stability assays

Firstly, the plasma stability of peptides was measured through high-performance liquid chromatography (HPLC) analysis. Briefly, peptides were prepared as solutions of 8, 4, 2, 1, 0.5, 0.25, 0.125, 0.0625 mM in deionized water, which were used to establish the standard curves using HPLC. Then, peptides were prepared as an 8 mM solution in water. Peptide solution (1 mL) was mixed with 25 % (*v*/*v*) blood plasma (3 mL) and then incubated at 37 °C for different time durations with constant agitation. At different time points, a mixture (50 μL) containing 90 % acetonitrile and 10 % TFA was dropped into the peptide/plasma solution (50 μL) to stop the further degradation. This solution was cooled to 4 °C and subsequently centrifuged at 10000 rpm for 10 min to separate the plasma proteins as a residue. The supernatant was used for HPLC analysis. Each sample was repeated in triplicate.

Subsequently, the plasma stability of peptides was evaluated by determining their MICs after different incubation periods with blood plasma. Briefly, peptide/PBS solutions were prepared at various concentrations (400, 200, 100, 50, 25, 12.5, 6.25 and 3.125 μM). 1.5 ml of blood plasma was mixed with 0.5 ml of peptide/PBS solution, and the mixture was incubated at 37 °C for different time durations with constant agitation. The mixtures at different time points were used for the MIC assay, the procedure of which was as mentioned above.

The salt sensitivity of the peptides was assessed by determining their MICs in the existence of different salts (150 mM NaCl, 4.5 mM KCl, 1 mM $MgCl_2$ and 4 μM $FeCl_3$). The procedure of MIC assay was as mentioned above.

Time-killing kinetics

The investigation of the time-killing kinetics of the peptides was conducted by counting the surviving bacterial cells treated with the peptides at different time points. Briefly, bacterial cells were treated with the peptides at the concentration of 2 × MIC. At specific time points (0, 30, 60, 120, 240, 360, and 1440 min), 20 uL of samples were collected, diluted serially, and plated on nutrient agar plates. The bacterial colonies were counted after 24 h of incubation at 37 °C. Each sample was repeated in triplicate. PBS and Polymyxin B served as negative and positive controls, respectively.

Synergistic effects of P-α-02-B with conventional antibiotics

The synergistic effects of P-α-02-B combined with conventional antibiotics levofloxacin or meropenem trihydrate were investigated by determining fractional inhibitory concentration index (FICI) through the checkerboard method. P-α-02-B and each antibiotic were mixed at the concentration of 2 × MIC, and subsequently two-fold serial dilutions were prepared in the broth medium. Subsequently, the above mixtures (50 μL) and diluted bacterial suspensions (50 μL, 1.0×10^6 CFU/mL) were added to each well of 96-well plates, followed by an incubation for 16 h at 37 °C. The following operations were performed as those of the MIC assay. FICI was defined and interpreted as follows: [23].

$$FICI = (\text{MIC of peptide in combination}) \,/\, (\text{MIC of peptide alone}) + (\text{MIC of antibiotic in combination}) \,/\, (\text{MIC of antibiotic alone}).$$

FICI ≥4: antagonism; 1.0 ≤ FICI < 4.0: indifference; 0.5 < FICI < 1: partial synergy; FICI ≤0.5: synergy.

Anti-biofilm activity

Firstly, we assessed the inhibition of biofilm formation. Briefly, the peptide solutions (100 μL) at various concentrations were added to a 96-well plate to mix with bacterial suspension (10 μL, 5×10^6 CFU/mL) in each well. The supernatant was removed after 24 h of incubation at 37 °C, three times of PBS washing followed. The biofilms were first treated with 100 % methanol for 20 min and then stained using 0.1 % crystal violet for another 20 min. After staining, the supernatant was removed, followed by PBS washing three times and air-drying. Then, 100 μL ethanol (95 %, *v*/*v*) was added into each well, followed by gentle shaking to dissolve the biofilms. Each sample was repeated in triplicate. The absorbance at 600 nm was measured with a SpectraMax M5 microplate reader (Molecular, USA). The broth medium without peptides was used as a control. Biofilm production rate was defined according to the following equation:

$$\text{Biofilm production rate (\%)} = OD_{Peptide} / OD_{Control} \times 100\ \%.$$

Subsequently, the disruption of the established biofilms was assessed. Briefly, bacterial suspensions (100 μL; 5.0×10^5 CFU/mL) were added into each well of a 96-well plate, followed by incubation at 37 °C for 24 h under static conditions to enable the formation of biofilms. After incubation, the established biofilms were treated with the peptide solutions for another 24 h. The following operations were performed as described above. Each sample was repeated in triplicate. The broth medium without peptides served as a control. Biofilm remaining rate was defined as follows:

$$\text{Biofilm remaining rate (\%)} = OD_{Peptide} / OD_{Control} \times 100\ \%.$$

Outer and inner membrane permeabilization assays

The peptide-induced bacterial outer membrane permeabilization was evaluated through the NPN assay. After being centrifuged at 1000 g for 10 min, *E. coli* ATCC 25922 bacterial cells were collected, washed three times with HEPES buffer (5 mM), and diluted to an OD_{600} of 0.5 in HEPES buffer. NPN (50 μL, 40 μM) was added to a 96-well black plate, subsequently the bacterial suspensions (100 μL) and different peptide solutions (50 μL) were added successively. Each sample was repeated in triplicate. The fluorescence (excitation at 350 nm and emission at 420 nm) was determined every 1 min over a 12-min period using a SpectraMax M5 microplate reader (Molecular, USA). HEPES served as a control.

The peptide-induced bacterial inner membrane permeabilization was evaluated by determining the intracellular activity of β-galactosidase. After being centrifuged at 1000 g for 10 min, *E. coli* ATCC 25922 bacterial cells were collected, washed three times with PBS, and diluted to an OD_{420} of 1.2 in PBS. ONPG (30 mM, 10 μL) was added to a 96-well transparent plate, subsequently the bacterial suspensions (90 μL) and different peptide solutions (100 μL) were added successively. Each sample was repeated in triplicate. The absorbance at 420 nm was measured every 5 min for a total duration of 135 min using a SpectraMax M5 microplate reader (Molecular, USA). PBS and 1 % Triton X-100 were used as negative and positive controls, respectively.

Transmission electron microscopy (TEM) assay

After being centrifuged at 1000 rpm for 10 min, *S. aureus* and *E. coli* ATCC 25922 bacterial cells were collected, washed three times with PBS, and resuspended to 1×10^8 CFU/mL. The bacterial cells were treated with $sC18_{4b}$ and P-α-02-B at the concentration of 2 × MIC at 37 °C with constant agitation for 2 h, and the bacterial cells treated with sterile broth served as the control. After treatment, the cells were harvested and post-processed for the final observation by TEM.

Confocal laser scanning microscopy (CLSM) assay

Bacterial cells were obtained after centrifugation at 1000 rpm for 10 min. They were washed three times using PBS and then re-suspended to 1×10^8 CFU/mL. The bacterial cells were treated with $sC18_{4b}$ and P-α-02-B at the concentration of 2 × MIC at 37 °C with constant agitation for 1 h, and the bacterial cells treated with sterile broth served as the control. Following another centrifugation at 1000 rpm for 10 min, the bacterial cells were gathered, washed three times with PBS, and then exposed to PI (20 μg/mL) for 10 min at 4°C in darkness. Then, the bacterial cells were centrifuged (1000 rpm, 10 min), washed three times with PBS, and exposed to DAPI (20 μg/mL) for 10 min at 4 °C in the dark. After centrifugation and PBS washing three times, the bacterial cells were resuspended in PBS. The suspensions were transferred to glass-bottom dishes for CLSM observation.

All-atom molecular dynamics (AAMD) simulations

The peptides $sC18_{4b}$ (GLRKRLRKFFNKIKF-NH_2) and P-α-02-B (Ac-GLZOWLZOFWNOIOZ-NH_2) were predicted by PEP-FOLD4. The YASARA software suite v.23.5.19 was employed to build the models and perform AAMD simulations [24]. To mimic the inner membrane (IM) of Gram-negative bacteria, asymmetric bilayer membrane composed of 75 % 1-palmitoyl-2-oleoyl phosphatidylethanolamine (POPE) and 25 % 1-palmitoyl-2-oleoyl phosphatidylglycerol (POPG) was constructed and neutralized with 0.9 % Na^+.

The AMBER14 force field, which is integrated into the YASARA suite, was utilized to refine the models. The simulation protocol involved optimizing the hydrogen bonding network to enhance the stability of the solutes [25], predicting the side-chain *p*Ka of each protein at pH 7.4 [26], and performing energy minimization to eliminate clashes using steepest descent and simulated annealing methods. Subsequently, the simulations were conducted using the AMBER14 force field for the solutes and the TIP3P water model. A 250 ps equilibration period was included in the YASARA MD simulation macro without an explicit equilibration step. A cutoff of 8 Å was applied to non-bonded real-space forces to ensure maximum accuracy, albeit at a higher computational cost. The Particle Mesh Ewald (PME) method was also employed [27]. The algorithms utilized in this study were described in detail in the literature [28], and the equations governing the motions were integrated using a multiple time-step of 1.25 fs for bonded and non-bonded interactions, simulating conditions at 298 K and 1 bar (NPT ensemble, analogous to a living cell environment). Periodic boundary conditions were implemented. Snapshots were saved every 100 ps, spanning a total simulation time of 50 ns. It is noteworthy that a longer simulation time was not feasible due to facility limitations.

Acute toxicity test

The acute toxicity of P-α-02-B was evaluated in normal mice. Briefly, 42 male Kunming mice (8 weeks old) were randomly

divided into 7 groups, and then intravenously injected with 100 μL of P-α-02-B (0, 2.5, 5, 10, 15, 20, and 25 mg/kg), the survival rate of mice was monitored within 5 days. In addition, 10 male Kunming mice (8 weeks old) were randomly divided into 2 groups, including the control group and the P-α-02-B group. The two groups of mice were intravenously injected with 100 μL saline and P-α-02-B (10 mg/kg), respectively. The body weights, behaviors, and survival status of each mouse were recorded every day throughout the experiment. The blood from eye socket was collected to prepare the whole blood and serum samples 7 days postinjection. Then the mice were executed, and the main organs were harvested for Hematoxylin and Eosin (H&E) staining.

In vivo antimicrobial assay

Male Kunming mice (8 weeks old) were obtained from Beijing Vital River Laboratory Animal Technology Co., Ltd. (Beijing, China). After environmental adaption for 1 week, all mice were intraperitoneally injected with cyclophosphamide (150 mg/kg for 96 h and 100 mg/kg for 24 h before bacterial infection, respectively) to induce the neutropenia. *S. aureus* (MDR) in saline (100 μL, 1×10^9 CFU/mL) was intraperitoneally injected into each mouse to establish a *S. aureus*-infected model.

2 H after the bacterial inoculation, the mice in administration groups (n = 8) were intravenously injected with 5 mg/kg P-α-02-B, 10 mg/kg P-α-02-B, 2.5 mg/kg levofloxacin, 5 mg/kg P-α-02-B combined with 2.5 mg/kg levofloxacin, and 10 mg/kg P-α-02-B combined with 2.5 mg/kg levofloxacin (100 μL) respectively. The mice in the saline group (n = 12) were treated with saline (100 μL). The mice in the control group (n = 6) were not inoculated with bacteria. 10 h after the bacterial inoculation, the second administration with the same dose was performed. The administration for each group were continued for three days with an interval of 24 h. The blood from eye socket was collected for bacterial count each day. 62 h after the bacterial inoculation, the mice were executed, then the main organs were harvested for H&E staining. The body weights and survival status of each mouse were recorded each day

All experimental procedures were conducted in accordance with the National Research Council's Guide for the Care and Use of Laboratory Animals, and were approved by the Animal Care and Use Committee of National Beijing Center for Drug Safety Evaluation and Research (IACUC-2023-002C).

Pharmacokinetics (PK)

Male SD rats (200 g ~ 220 g) were obtained from Beijing Vital River Laboratory Animal Technology Co., Ltd. (Beijing, China). The rats (n = 6) were injected intravenously (10 mL/kg) with P-α-02-B dissolved in normal saline (1 mg/mL). Blood samples were harvested into heparin tubes at 2, 5, 15, 30 min, and 1, 2, 4, 6 h after administration. The blood samples were centrifuged to obtain plasma, and then precipitated with acetonitrile to remove proteins. The concentration of P-α-02-B was monitored by an LC-MS/MS system. The quantitative range for P-α-02-B for this experiment is 25 ng/mL ~ 5000 ng/mL. Samples above this range were diluted with plasma for testing, while samples below this range were denoted as BLQ (below the limit of quantitation). The main pharmacokinetic parameters were calculated using WinNonlin software and a non-compartmental model.

Statistical analysis

All data in this study were presented as mean ± SD. The statistical differences between different groups were determined by one-way analysis of variance (ANOVA). *P*-Values less than 0.05, 0.01, and 0.001 were statistically significant.

Results and discussion

Design, synthesis and characterization of AMPs

$sC18_{4b}$ is a cationic amphipathic AMP with broad-spectrum antimicrobial activity, which kills bacteria mainly through membrane-disruption [29]. To improve the antimicrobial activity and stability of the lead peptide $sC18_{4b}$, a series of $sC18_{4b}$ analogues were designed and synthesized (Table 1). $sC18_{4B}$ was obtained by the N-terminal acetylation of $sC18_{4b}$, which was reported to be effective in improving the antimicrobial activity and stability of AMPs [30,31]. For double-faced amphipathic AMPs, it is an effective strategy to enhance their antimicrobial activity by increasing their hydrophobicity and hydrophobic moments within limits [32,33]. Given the helical wheel projections shown in Fig. 1, $sC18_{4B}$ was anticipated to adopt a double-faced amphipathic α-helical secondary structure, which served as the structural basis for its antimicrobial effect [34]. In order to obtain AMPs with higher hydrophobicity and hydrophobic moments, $sC18_{4B}$ analogues (P-α, P-β, P-γ) were designed by increasing the hydrophobicity of the hydrophobic face separately or increasing the hydrophilicity and hydrophobicity of the corresponding faces simultaneously. For $sC18_{4B}$, the hydrophilic Arg at position 5 and the hydrophobic Phe at position 15 located at its hydrophobic and hydrophilic faces, respectively. P-α was designed by exchanging the positions of the above two amnio acids with each other, thus increasing the hydrophilicity and hydrophobicity of the hydrophilic and hydrophobic faces, respectively. P-β was designed by substituting the Arg at position 3 of P-α with Phe. Similarly, P-γ was designed by substituting the Lys at position 12 of P-β with Phe. Compared with P-α, P-β and P-γ presented incrementally enlarged hydrophobic surfaces and hydrophobicity.

Besides, different hydrophobic amino acids (Val, Trp, Ile, Leu, Ala, Met) were chosen to substitute the Phe at positions 5 and 10 of P-α, and consequently P-α-01 ~ P-α-06 with varied hydrophobicity were obtained. Similar to P-α-02, P-β-02 was obtained by substituting the Phe at positions 3, 5 and 10 of P-β with Trp. To enhance the stability of P-α-02 and P-α-04, unnatural amino acids were incorporated into them. To be specific, homoarginine was chosen to substitute Arg to obtain P-α-02-X and P-α-04-X, and ornithine was chosen to substitute Lys to obtain P-α-02-O and P-α-04-O. In addition, P-α-02-B and P-α-04-B were designed by substituting Arg and Lys with homoarginine and ornithine respectively, and P-α-04-A was designed by substituting both Arg and Lys with homoarginine. P-α-02-D and P-α-02-D' were D-type isomers of P-α-02, with Ile of two different configurations. The purity of the peptides was confirmed to be > 95 % (Fig. S1). The molecular weights (MWs) of the peptides were confirmed to be correct (Fig. S2).

According to previous reports, the secondary structures of AMPs, such as α-helix and β-sheet conformations, are essential in dictating their membrane permeabilization [35]. Besides, the α-helical structure can improve the ability of AMPs to resist enzymatic hydrolysis, thus increasing their half-lives and enhancing their antimicrobial effects [36,37]. Therefore, we investigated the secondary structures of $sC18_{4b}$ and $sC18_{4b}$ analogues in TFE/PBS (50 %, *v*/*v*) solution, which could mimic the environment of the membrane. The CD spectra showed the characteristic absorption bands at wavelengths of 208 nm and 222 nm (Fig. 2), suggesting that each of the peptides adopted an α-helical conformation in TFE. As expected, due to being composed of D-type amino acids, the D-type peptides (P-α-02-D, P-α-02-D') exhibited opposite

Table 1
Sequences and key physicochemical parameters of $sC18_{4b}$ and its analogues.

Compounds	Sequences[a]	MWs		t_R[b] (min)	Hydrophobic moment[c] (μH)
		calculated	measured		
$sC18_{4b}$	GLRKRLRKFFNKIKF-NH2	1950.43	1949.821	10.473	0.561
$sC18_{4B}$	Ac-GLRKRLRKFFNKIKF-NH2	1992.46	1991.265	11.243	0.561
P-α	Ac-GLRKFLRKFFNKIKR-NH2	1992.46	1991.267	12.041	0.784
P-β	Ac-GLFKFLRKFFNKIKR-NH2	1983.45	1983.015	13.284	0.800
P-γ	Ac-GLFKFLRKFFNFIKR-NH2	2002.45	2001.567	14.654	0.784
P-α-01	Ac-GLRKVLRKFVNKIKR-NH2	1896.38	1895.800	11.185	0.758
P-α-02	Ac-GLRKWLRKFWNKIKR-NH2	2070.53	2069.809	12.047	0.805
P-α-03	Ac-GLRKILRKFINKIKR-NH2	1924.43	1923.890	11.943	0.785
P-α-04	Ac-GLRKLLRKFLNKIKR-NH2	1924.43	1923.866	12.246	0.780
P-α-05	Ac-GLRKALRKFANKIKR-NH2	1840.27	1839.806	10.496	0.717
P-α-06	Ac-GLRKMLRKFMNKIKR-NH2	1960.51	1959.805	11.650	0.759
P-β-02	Ac-GLWKWLRKFWNKIKR-NH2	2100.56	2099.708	11.982	0.827
P-α-02-X	Ac-GLZKWLZKFWNKIKZ-NH2	2112.68	2111.758	11.835	N/A
P-α-02-O	Ac-GLROWLROFWNOIOR-NH2	2014.37	2013.701	12.049	N/A
P-α-02-B	Ac-GLZOWLZOFWNOIOZ-NH2	2056.52	2055.254	12.050	N/A
P-α-02-D	Ac-glrkwlrkfwnkikr-NH2	2070.53	2069.384	11.800	N/A
P-α-02-D'	Ac-glrkwlrkfwnki'kr-NH2	2070.53	2069.731	12.209	N/A
P-α-04-X	Ac-GLZKLLZKFLNKIKZ-NH2	1966.58	1967.402	11.951	N/A
P-α-04-O	Ac-GLROLLROFLNOIOR-NH2	1868.27	1867.807	6.220	N/A
P-α-04-B	Ac-GLZOLLZOFLNOIOZ-NH2	1910.42	1910.363	12.673	N/A
P-α-04-A	Ac-GLZZLLZZFLNZIZZ-NH2	2134.75	2133.897	13.158	N/A

[a] D-type amino acids are represented by lower-case letters (i: D-type Ile, i': D-type Allo-Ile); homoarginine and ornithine are represented by letter Z and letter O, respectively.
[b] The retention time (t_R) on HPLC of each peptide was positively correlated with its hydrophobicity.
[c] The hydrophobic moment of the peptide, which was positively correlated with its amphipathicity, was calculated via *Heliquest* (http://heliquest.ipmc.cnrs.fr/cgi-bin/ComputParams.py). Due to site limitations, the hydrophobic moment of the peptides containing unnatural amino acids cannot be calculated.

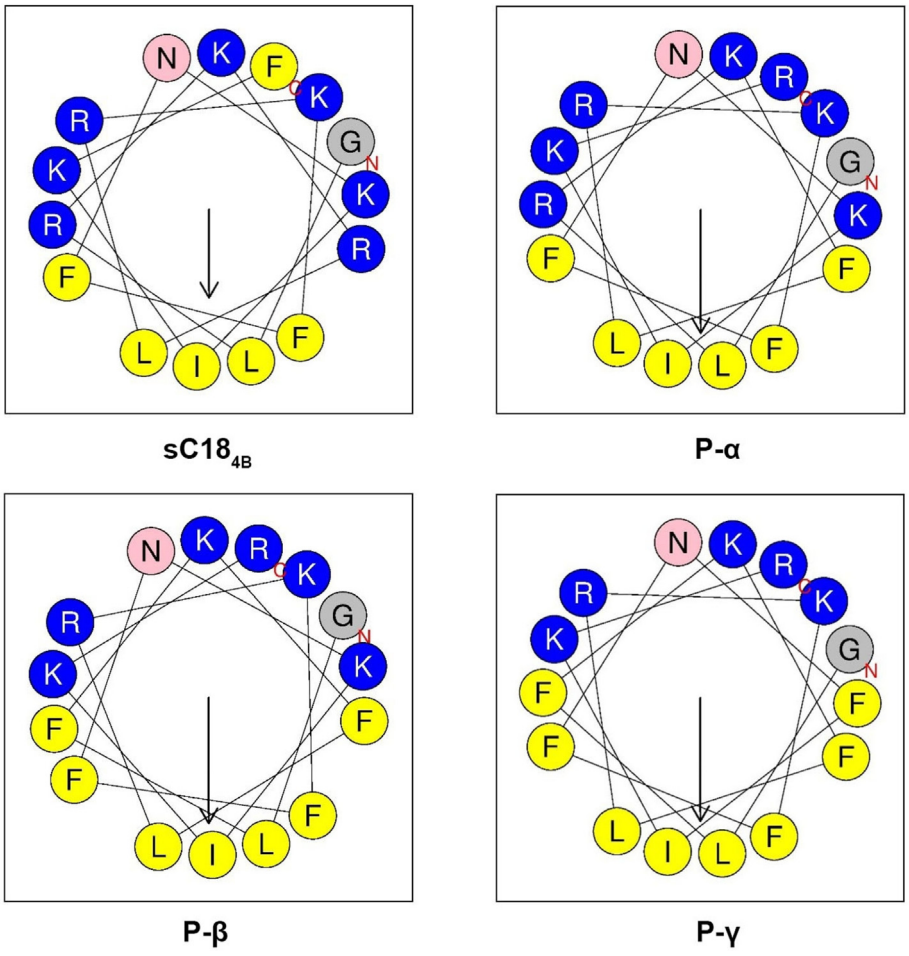

Fig. 1. The helical wheel projections of $sC18_{4B}$, P-α, P-β and P-γ, as predicted via *HeliQuest* (http://heliquest.ipmc.cnrs.fr/cgi-bin/ComputParams.py). The hydrophobic amino acids on the hydrophobic face of the helix are colored in yellow, the hydrophilic amino acids on the hydrophilic face of the helix are colored blue. The neutral Asn and Gly are colored red and grey, respectively. The overall hydrophobic moment (μH) of the peptides is depicted by the arrow.

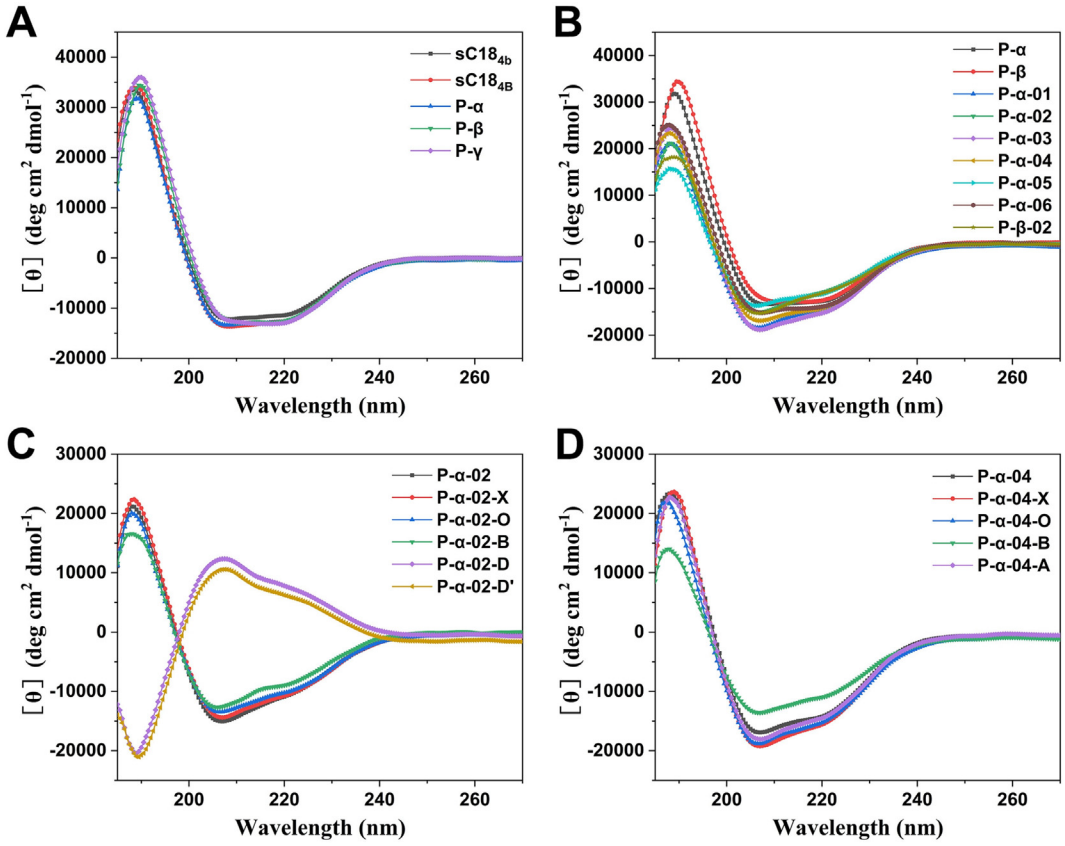

Fig. 2. The CD spectra of sC18$_{4b}$ (A), P-α and P-β (B), P-α-02 (C), P-α-04 (D) and their corresponding peptide analogues at 50 μM in 50 % TFE/PBS.

α-helical conformations compared with the corresponding L-type one (P-α-02).

Antimicrobial activity

The antimicrobial activity of all the peptides was assessed by determining their MICs against seven bacterial strains (Table 2). These sC18$_{4b}$ analogues showed appreciable antimicrobial activity against all the bacterial strains tested.

As mentioned above, the positive charges, hydrophobicity and hydrophobic moment of AMPs have notable effects on their antimicrobial activity. Compared with sC18$_{4b}$, the antimicrobial activity of N-terminal acetylated sC18$_{4B}$ barely changed, which may be due to the slightly changed positive charges and hydrophobicity, and the unchanged hydrophobic moment. After amino acid exchange and substitution, three sC18$_{4B}$ analogues including P-α, P-β and P-γ, which possessed incrementally enlarged hydrophobic surfaces, were obtained. P-α possessed higher hydrophobicity and hydrophobic moment compared with sC18$_{4B}$, the antimicrobial activity of it increased as expected. To be specific, P-α presented a 2-fold reduction in MICs against all the bacterial strains tested except for *B. subtilis* ATCC 6633. Despite the higher hydrophobicity and hydrophobic moment, P-β did not exhibit higher antimicrobial activity compared with P-α, which could be attributed to the decreased positive charges [38]. It could also be explained that the hydrophobicity of P-β may be out of the limit for its optimum antimicrobial activity, which was proven through P-γ subsequently. P-γ showed a significant loss in antimicrobial activity compared with P-β, which was likely attributed to its excessively high hydrophobicity and decreased positive charges. The results suggested that the high antimicrobial potency of AMPs largely depended on proper hydrophobic properties and positive charges.

Given the enhanced antimicrobial activity of P-α, six P-α analogues (P-α-01 ∼ P-α-06) were obtained by substituting the Phe at positions 5 and 10 with different hydrophobic amino acids. These analogues possessed equivalent positive charges, different hydrophobic moments and varied hydrophobicity. Compared with P-α, the antimicrobial activity of P-α-02, P-α-03 and P-α-04 improved to varying degrees, while that of P-α-01, P-α-05 and P-α-06 showed significant reduction. Among them, P-α-02 and P-α-04 showed the highest antimicrobial activity. Notably, the relative antimicrobial activity of P-α and P-α-01 ∼ P-α-06 was positively related to their hydrophobicity except for P-α-03, which indicated that the relative antimicrobial activity between these peptides was mainly correlated with their hydrophobicity. It was reported that the amphipathic indole side chain in Trp was able to anchor the lipid bilayers through the hydrogen bond and hydrophobic interaction [33]. Therefore, the introduction of Trp into AMPs is an efficacious strategy to mediate the interaction between AMPs and bacterial cell membranes, thus promoting the membrane disruption by AMPs. However, P-β-02 exhibited a lower antimicrobial activity compared to P-β, which could be attributed to the decreased hydrophobicity.

Subsequently, different unnatural amino acids were incorporated into P-α-02 and P-α-04. Given the results of MIC assays, the antimicrobial activity of P-α-02-X and P-α-02-B against *A. baumannii* was higher than that of P-α-02, their antimicrobial activity against the other five bacterial strains remained unchanged. Compared with P-α-04, the antimicrobial activity of P-α-04-X, P-α-04-O, P-α-04-B and P-α-04-A against *E. aerogenes* was lower than that of P-α-04, their antimicrobial activity against the other five bacterial strains remained unchanged. Overall, the introduction of unnatural amino acids could enhance the antimicrobial activity of P-α-02 analogues, but failed to enhance that of P-α-04

Table 2
MICs of $sC18_{4b}$ and its analogues against bacterial strains.

Compounds	MIC (μM)					
	Gram-positive bacteria		Gram-negative bacteria			
	B. subtilis ATCC 6633	*S. aureus* (MDR)	*E. coli* ATCC 25,922	*E. aerogenes* (MDR)	*A. baumannii* (MDR)	*C. freundii* (MDR)
$sC18_{4b}$	6.25	12.5	12.5	12.5	12.5	12.5
$sC18_{4B}$	6.25	12.5	12.5	25	12.5	12.5
P-α	6.25	6.25	6.25	12.5	6.25	6.25
P-β	6.25	6.25	6.25	12.5	6.25	6.25
P-γ	12.5	50	12.5	50	12.5	50
P-α-01	6.25	25	12.5	50	12.5	6.25
P-α-02	3.125	3.125	3.125	6.25	6.25	3.125
P-α-03	3.125	6.25	3.125	12.5	6.25	6.25
P-α-04	3.125	3.125	3.125	6.25	6.25	3.125
P-α-05	25	50	50	50	50	50
P-α-06	6.25	12.5	12.5	25	12.5	6.25
P-β-02	6.25	25	12.5	25	12.5	12.5
P-α-02-X	3.125	3.125	3.125	6.25	3.125	3.125
P-α-02-O	3.125	3.125	6.25	12.5	3.125	3.125
P-α-02-B	3.125	3.125	3.125	6.25	3.125	3.125
P-α-02-D	3.125	3.125	3.125	6.25	6.25	3.125
P-α-02-D'	3.125	3.125	3.125	6.25	6.25	3.125
P-α-04-X	3.125	3.125	3.125	12.5	6.25	3.125
P-α-04-O	3.125	3.125	3.125	25	6.25	3.125
P-α-04-B	3.125	3.125	3.125	12.5	6.25	3.125
P-α-04-A	3.125	3.125	3.125	12.5	6.25	3.125
Polymyxin B	1.56	25	0.78	1.56	0.78	1.56

analogues. The D-type isomers of P-α-02 (P-α-02-D and P-α-02-D') showed unchanged antimicrobial activity compared with P-α-02, suggesting that the configuration had no significant effect on their antimicrobial activity. Of the above 9 unnatural amino acid-containing peptide analogues, the homoarginine containing ones showed stronger antimicrobial activity than those without homoarginine, indicating that the strategy of homoarginine substitution was more effective in the improvement of antimicrobial activity.

We calculated the GM of MICs against all (GM_{all}), Gram-positive (GM^+) and Gram-negative (GM^-) bacteria of the peptides (Table 3). Interestingly, the GM^+ values of $sC18_{4b}$ and $sC18_{4b}$ analogues were less than the GM^- values of them. Notably, P-α-02-B had the lowest GM_{all}, demonstrating P-α-02-B showed potent antimicrobial activity against both Gram-positive and Gram-negative bacteria.

Hemolysis and cytotoxicity analysis

A low toxicity towards mammalian cells is a prerequisite for AMPs used in clinical applications. Therefore, the hemolysis and cytotoxicity of $sC18_{4b}$ and some of its analogues were evaluated using 5 % (*v*/*v*) hRBCs (Fig. 3). The HC_{50} values and SIs were calculated and utilized to indicate the hemolytic activity and antimicrobial selectivity of the peptides (Table 3). In comparison with $sC18_{4B}$ (HC_{50} = 471.41 μM), P-α (HC_{50} > 1000 μM) showed decreased hemolytic activity, while P-β (HC_{50} = 136.69 μM) showed increased hemolytic activity. Even at the highest tested concentration (50 μM), the percentage of hemolysis of P-α was negligible (1.5 %). Besides, P-α showed superior antimicrobial selectivity (SI > 1000). Compared with P-α, P-α-04 and its analogues still maintained low hemolytic activity and high antimicrobial selectivity, while P-α-02 and its analogues showed increased hemolytic activity and decreased antimicrobial selectivity.

The evaluation of peptide cytotoxicity was performed in the 293 T cell line at concentrations from 0.78 to 50 μM. Compared with $sC18_{4B}$, P-α showed slightly lower cytotoxicity (the CC_{50} of P-α could not be obtained based on existing data), while P-β showed much higher cytotoxicity. The increased hemolytic activity and cytotoxicity of P-β could be attributed to its increased hydrophobicity [39,40]. Compared with P-α, the cytotoxicity of P-α-02 obviously increased, while that of P-α-04 still maintained at a low level (CC_{50} = 192.76). Among P-α-02 and its analogues, P-α-02-B showed the lowest cytotoxicity (CC_{50} = 43.06). In contrast, all P-α-04 analogues showed significantly increased cytotoxicity compared with P-α-04, thus being excluded from the following assessments. Compared with P-α-02, its D-type isomers (P-α-02-D and P-α-02-D') showed increased hemolytic activity and cytotoxicity. Therefore, P-α-02-D and P-α-02-D' were not chosen for the following assessments.

Plasma and salt stability

The poor stability hindered the clinical applications of AMPs *in vivo*, we therefore introduced unnatural amino acids to improve the plasma stability of the peptides. To test the plasma stability of P-α-02 and its peptide analogues (P-α-02-X, P-α-02-O, P-α-02-B), the peptides were first incubated with human plasma (25 %, *v*/*v*) for various durations (0 h, 3 h, 6 h, 9 h, 12 h, 24 h, 48 h) at 37 °C before being analyzed by HPLC (Fig. 4). The half-lives of the peptides in plasma were calculated using SPSS software (Table S1), revealing the following stability order: P-α-02 < P-α-02-O < P-α-02-X < P-α-02-B. The results demonstrated that the introduction of unnatural amino acids significantly enhanced the plasma stability of P-α-02. After 48 h of incubation, 83.07 % of P-α-02-B remained intact, demonstrating that P-α-02-B was highly-resistant to the plasma digestion. In contrast, the percentages of residual P-α-02, P-α-02-O and P-α-02-X were less than 20 % (Fig. 4C). To further evaluate the stability of P-α-02-B, we performed a long-term plasma stability assay. As shown in Fig. 4D, 53.19 % of P-α-02-B remained intact after being treated with plasma for 14 days, which further confirmed its high resistance to the plasma digestion. Additionally, we evaluated the plasma stability of P-α and P-α-04 within 24 h. Compared with P-α-02-B ($t_{1/2}$ = 234.57h), P-α ($t_{1/2}$ = 15.28 h) and P-α-04 ($t_{1/2}$ = 17.42 h) showed much lower plasma stability (Fig. S3), indicating that they could be more readily degradable *in vivo*.

Besides, the stability of the peptides was assessed by pretreating the peptides with plasma for different durations (6 h and 12 h) at 37 °C before determining their MICs against *S. aureus*

Table 3
HC_{50}, GM, and SI values of some $sC18_{4b}$ analogues.

Compounds	HC_{50} (μM)	CC_{50}	GM_{all} (μM)	SI_{all}	Gram-positive bacteria		Gram-negative bacteria	
					GM^+ (μM)	SI^+	GM^- (μM)	SI^-
$sC18_{4B}$	471.41	351.6	12.5	37.71	8.84	53.33	12.50	37.71
P-α	>1000	N/A	7.02	>1000	6.25	>1000	14.87	>1000
P-β	136.69	28.20	7.02	19.48	6.25	21.87	7.43	18.39
P-α-02	156.00	36.72	3.94	39.62	3.13	49.92	7.43	20.99
P-α-04	>1000	192.76	3.94	>1000	3.13	>1000	4.42	>1000
P-α-02-X	106.72	30.97	3.51	30.42	3.13	34.15	4.42	24.15
P-α-02-O	184.17	20.53	4.42	41.67	3.13	58.93	3.72	49.56
P-α-02-B	183.59	43.06	3.51	52.34	3.13	58.75	5.26	34.93
P-α-02-D	79.21	3.75	3.94	20.12	3.13	25.35	3.72	21.31
P-α-02-D'	119.75	3.41	3.94	30.41	3.13	38.32	4.42	27.10
P-α-04-X	451.73	12.41	4.42	102.21	3.13	144.55	4.42	102.21
P-α-04-O	>1000	17.77	4.96	495.70	3.13	786.88	5.26	467.88
P-α-04-B	>1000	7.24	4.42	>1000	3.13	>1000	6.25	>1000
P-α-04-A	>1000	5.04	4.42	818.06	3.13	>1000	5.26	687.90

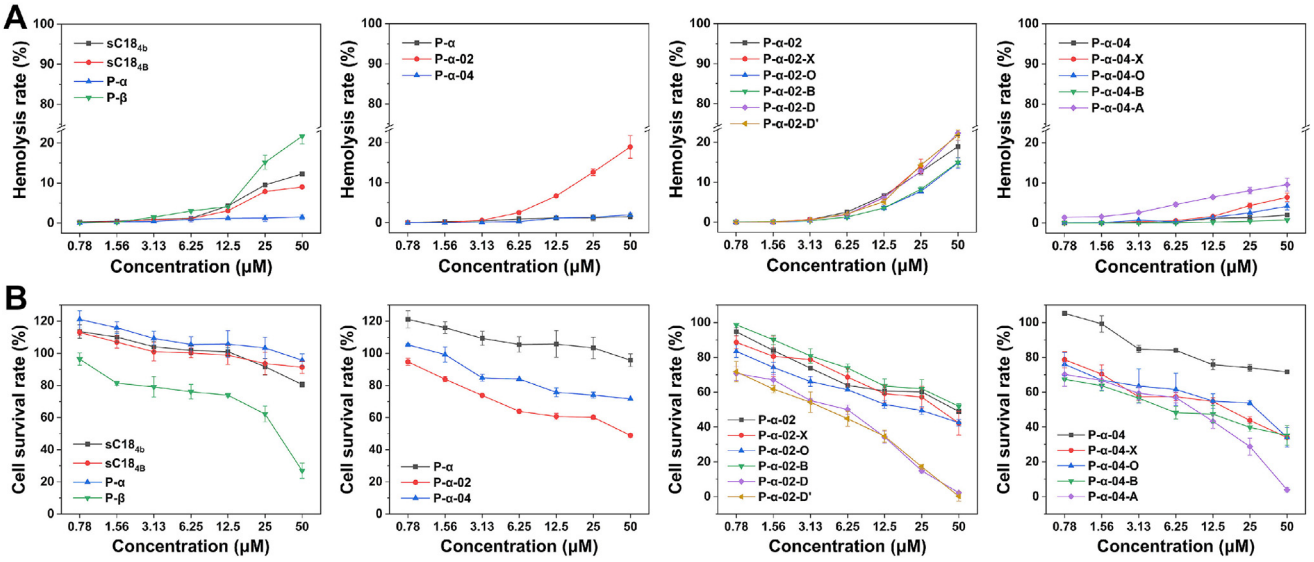

Fig. 3. Toxicity towards mammalian cells of $sC18_{4b}$ and its analogues. (A) Hemolytic activity of $sC18_{4b}$ and its analogues on hRBCs; (B) Cytotoxicity of $sC18_{4b}$ and its analogues against 293 T cells. The data are shown as mean ± standard deviation (SD) (n = 5).

and *E. coli* ATCC 25922. When the MIC of a peptide increased after the plasma pretreatment, the peptide was thought to undergo degradation. As shown in Fig. 4E and F, the four peptides all showed obvious bacterial inhibition effects before the plasma pretreatment. However, following the pretreatment with plasma, only P-α-02-B remained unchanged antimicrobial activity, while P-α-02, P-α-02-X and P-α-02-O all lost their antimicrobial activity in varying degrees. After 12 h of incubation, the MICs of P-α-02, P-α-02-O and P-α-02-X against both *S. aureus* and *E. coli* ATCC 25922 increased 16-fold, 4-fold and 2-fold, respectively. The results revealed the same stability order with that of the above HPLC assays (P-α-02 < P-α-02-O < P-α-02-X < P-α-02-B), which further demonstrated that the unnatural amino acid substitution strategy enhanced the stability of AMPs. Notably, after 12 h of incubation, the MICs of homoarginine containing peptides P-α-02-X (6.25 μM) and P-α-02-B (3.13 μM) against both *S. aureus* and *E. coli* ATCC 25922 remained at a low level, while that of P-α-02-O (25 μM) without homoarginine increased significantly. It indicated that the homoarginine containing peptides are more likely to maintain their antimicrobial activity in the presence of plasma than those without homoarginine. Thus, the strategy of homoarginine substitution in P-α-02 was more effective in the improvement of plasma stability.

To assess the salt sensitivity of P-α-02-B, the MICs of P-α-02-B against *S. aureus* and *E. coli* ATCC 25922 in the existence of various salts were evaluated. As shown in Table S2, P-α-02-B showed negligible changes in MIC values except for a four-fold increase against *S. aureus* in the NaCl solution. Compared with $sC18_{4B}$ and Polymyxin B, P-α-02-B showed stronger resistance to the interference caused by various salts. In summary, the combination strategy of regulating hydrophobic properties and introducing unnatural amino acids could simultaneously enhance the antimicrobial activity, bacterial selectivity, plasma stability, and salt stability of AMPs. Given the good and balanced performance of P-α-02-B in antimicrobial activity, hemolysis, cytotoxicity and stability assays, it was chosen for further evaluation in the following experiments.

Time-killing kinetics analysis

To evaluate the bacterial killing efficiency of $sC18_{4B}$ and P-α-02-B, a time-killing kinetic assay was carried out. Polymyxin B served as a positive control. $sC18_{4B}$, P-α-02-B, and Polymyxin B showed time-dependent bactericidal activity against both *S. aureus* and *E. coli* ATCC 25922 at the concentration of 2 × MIC (Fig. 5A and B). The bacterial killing efficiency order against *S. aureus* was as follows: Polymyxin B < $sC18_{4B}$ < P-α-02-B. Notably, P-α-02-B

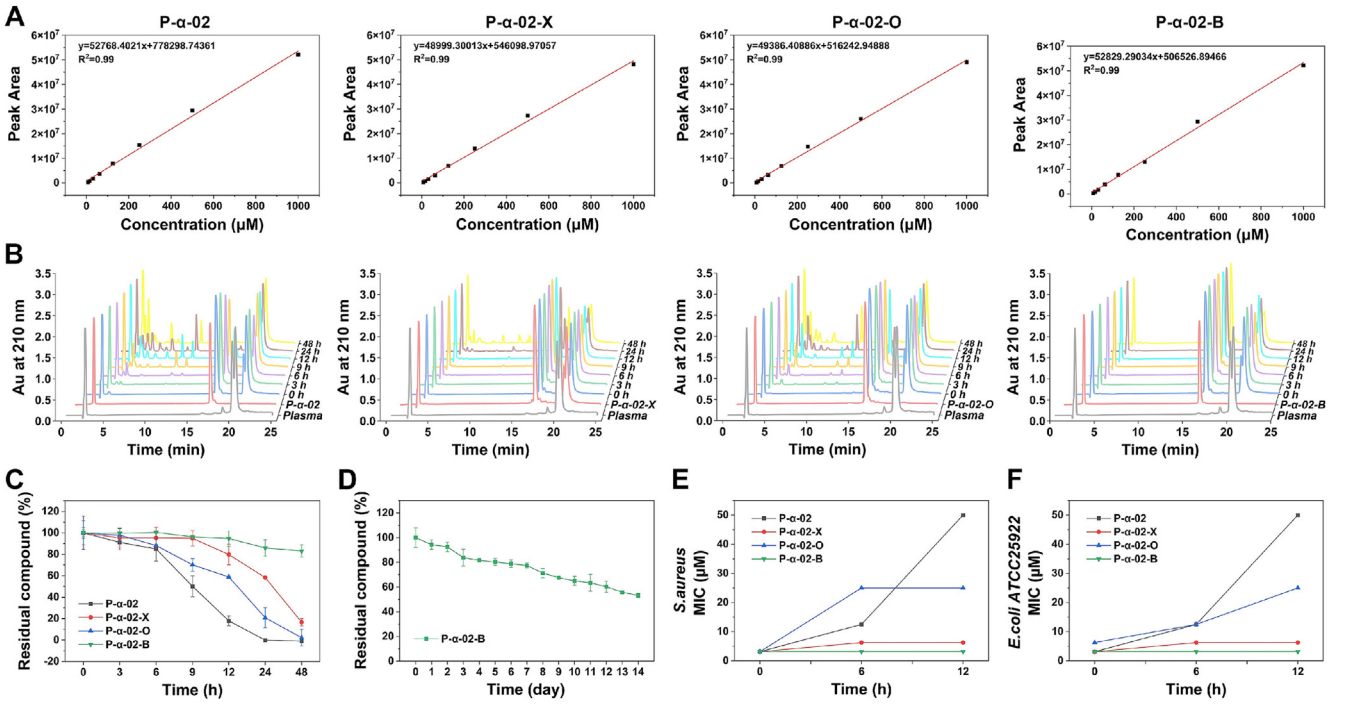

Fig. 4. Plasma stability of P-α-02 and its analogues. (A) Relationship between the peptide concentration of P-α-02, P-α-02-X, P-α-02-O and P-α-02-B and the corresponding peak area at 210 nm in HPLC; (B) Degradation chromatogram of P-α-02, P-α-02-X, P-α-02-O and P-α-02-B in plasma determined by HPLC; (C) Residual compounds of P-α-02, P-α-02-X, P-α-02-O and P-α-02-B after being treated with plasma for 0, 3, 6, 9, 12, 24 and 48 h; (D) Residual compounds of P-α-02-B after being treated with plasma for 0 ∼ 14 day; MIC values of P-α-02, P-α-02-X, P-α-02-O and P-α-02-B against *S. aureus* (E) and *E. coli* ATCC 25922 (F) after being treated with plasma for 0, 6 and 12 h. The data are shown as mean ± SD (n = 3).

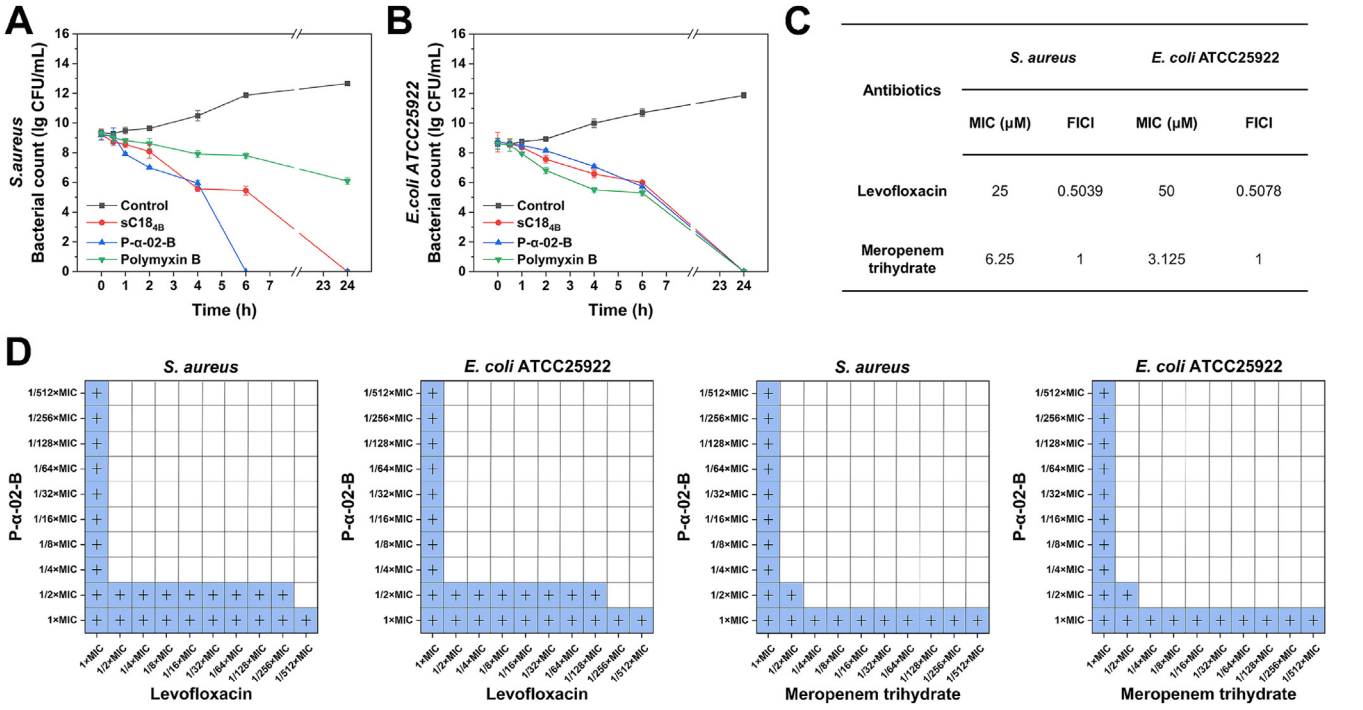

Fig. 5. Time-killing kinetics and synergistic antimicrobial effects analysis. Time-killing curves of $sC18_{4B}$, P-α-02-B and polymyxin B at the concentration of 2 × MIC against *S. aureus* (A) and *E. coli* ATCC 25922 (B). The data are shown as mean ± SD (n = 3); (C) MICs of antibiotics against *S. aureus* and *E. coli* ATCC 25922 and FICI of P-α-02-B combined with antibiotics; (D) Synergistic effects of P-α-02-B combined with levofloxacin or meropenem trihydrate against *S. aureus* and *E. coli* ATCC 25922 using checkerboard method. "+" represents the growth of bacteria was inhibited.

completely killed *S. aureus* within 6 h. As for *E. coli* ATCC 25922, $sC18_{4B}$, P-α-02-B, and Polymyxin B showed similar bacterial killing efficiency.

Synergistic Effects of P-α-02-B with Conventional Antibiotics

According to previous reports, AMPs combined with conventional antibiotics could outperform separate drugs in terms of antimicrobial effects [41–43]. For instance, quinolones kill bacteria mainly through inhibiting the synthesis of DNA and RNA. When the quinolone antibiotic is combined with AMPs, the membrane disruption effects of AMPs make it get easier access to the cytoplasm, thus improving its antimicrobial effects [44]. Besides, it was confirmed that AMPs and β-lactams could act synergistically, which may be correlated with their combined effects on bacterial cell envelopes [45–47]. We therefore evaluated the synergistic effects of P-α-02-B with levofloxacin (quinolones) or meropenem trihydrate (β-lactams) against *S. aureus* and *E. coli* ATCC 25922 through the checkerboard method (Fig. 5D).

As shown in Fig. 5C, P-α-02-B demonstrated partial synergistic activity against *S. aureus* and *E. coli* ATCC 25922 when combined with levofloxacin, with FICI values of 0.5039 and 0.5078, respectively. It was presumably due to their mutually complementary antibacterial mechanisms. FICI = 1 was determined for the combination of P-α-02-B and meropenem trihydrate, demonstrating no synergistic effect between them.

Anti-biofilm effects of P-α-02-B

Bacterial cells in biofilms are difficult to eradicate by using conventional antibiotics, thus making the treatment of biofilm-caused bacterial infections extremely challenging. Recently, AMPs were reported to not only inhibit the biofilm formation but also eradicate the established biofilms [48,49]. Therefore, we investigated

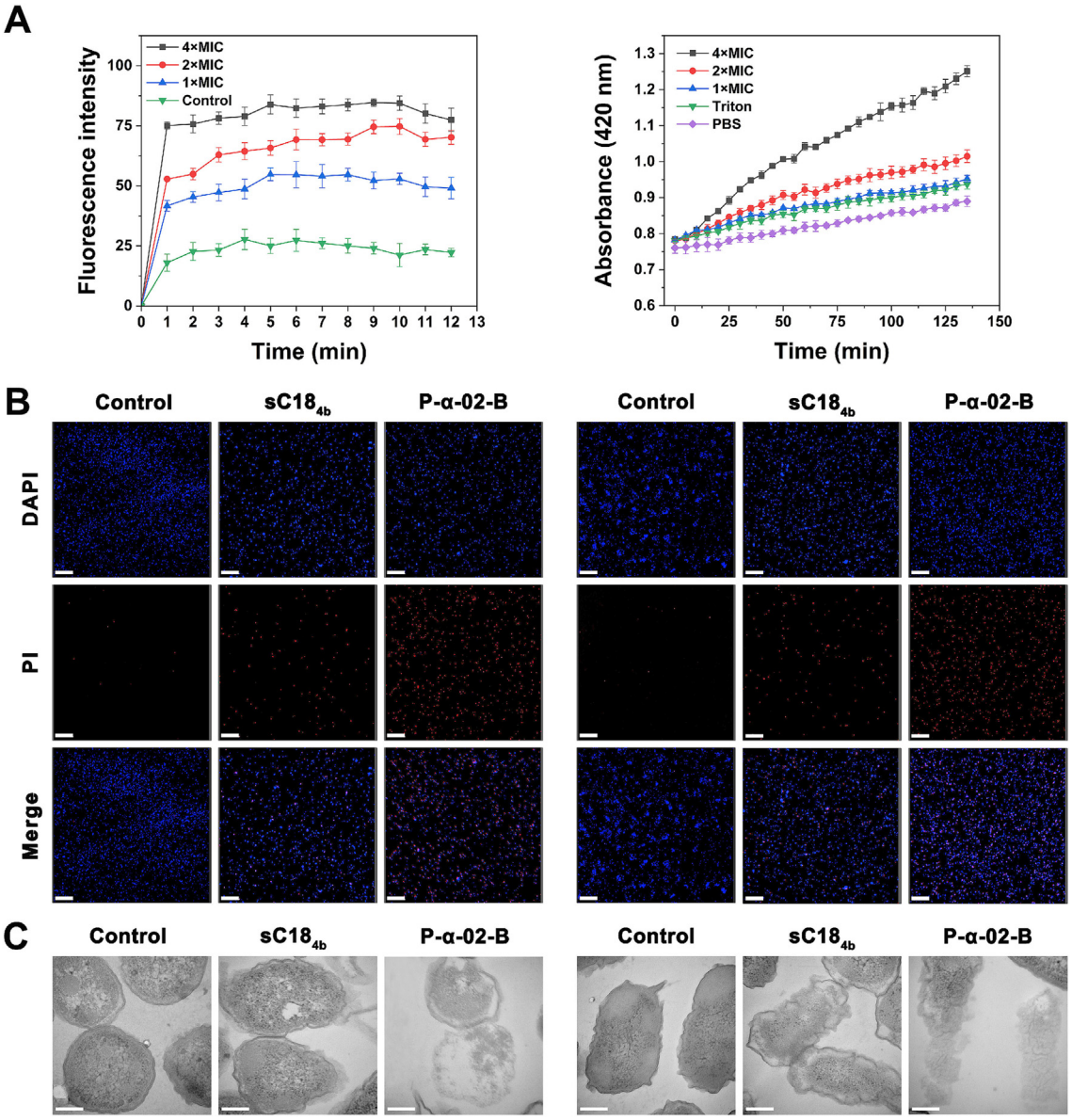

Fig. 6. The mechanism of action on bacterial membranes of P-α-02-B. (A) Effects of P-α-02-B on the permeabilization of the outer (left) and inner (right) membrane of *E. coli* ATCC 25922 cells. The data are shown as mean ± SD (n = 3); (B) CLSM images of *S. aureus* (left) and *E. coli* ATCC 25922 (right) bacterial cells treated with $sC18_{4b}$ and P-α-02-B at concentrations of 1 × MIC, 2 × MIC and 4 × MIC. The scale bar represents 70 μm; (C) TEM images of *S. aureus* (left) and *E. coli* ATCC 25922 (right) cells before and after being treated with $sC18_{4b}$ and P-α-02-B at the concentration of 2 × MIC for 2 h. The scale bar represents 200 nm.

the ability of P-α-02-B to inhibit biofilm formation and to disrupt established biofilms. As shown in Fig. S4A, P-α-02-B could inhibit biofilm formation in a dose-dependent manner. At the concentration of 4 × MIC, P-α-02-B inhibited the biofilms formed by *S. aureus* and *E. coli* ATCC 25922 by up to 42.85 % and 61.93 %, respectively. Besides, P-α-02-B could effectively disrupt the established biofilms (Fig. S4B). P-α-02-B killed more than 50 % of the live *S. aureus* and *E. coli* ATCC 25922 cells inside the biofilms at the lowest tested concentration (1/2 × MIC).

Mode of action studies

To assess the antimicrobial mechanism of P-α-02-B, the outer and inner membrane permeabilization assays were performed. Firstly, NPN was used to test the ability of P-α-02-B to disrupt or perturb outer bacterial membranes. NPN, which functions as a hydrophobic fluorescent probe, exhibited weak fluorescence when in a hydrophilic environment and strong fluorescence when in a hydrophobic one. When the outer bacterial membrane was disrupted, NPN could insert into the hydrophobic lipid membranes and exhibited increased fluorescence intensity [50]. As shown in Fig. 6A (left), the fluorescence intensity of NPN showed a rapid increase within 1 min in a dose-dependent manner. It suggested that P-α-02-B could increase the outer membrane permeability through membrane disruption in a short time.

Subsequently, the inner membrane permeabilization of P-α-02-B was assessed with ONPG as a fluorescence substrate. Once the inner bacterial membrane was disrupted, the ONPG was able to interact with the intracellular β-galactosidase, and subsequently, a change in fluorescence occurred [51]. As shown in Fig. 6A (right), P-α-02-B led to inner membrane permeabilization in a time- and dose-dependent manner, the process of which was relatively slow. At the concentration of 1 × MIC, the inner membrane permeabilization of bacterial cells treated with P-α-02-B was slightly stronger than that of positive control (1 % Triton X-100), suggesting that P-α-02-B was highly-effective in disrupting the integrity of inner membranes.

To verify the membrane disruption mechanism of the peptides, the *S. aureus* and *E. coli* ATCC 25922 bacterial cells were stained with DAPI and PI, treated with $sC18_{4b}$ and P-α-02-B, and observed with CLSM. DAPI stains all bacterial cells blue, irrespective of the integrity of their membranes, while PI only stains those with disrupted membranes red. As shown in Fig. 6B, the untreated *S. aureus* and *E. coli* ATCC 25922 bacterial cells showed strong blue fluorescence but almost no red fluorescence. In the experimental groups, the bacterial cells treated with $sC18_{4b}$ showed strong blue fluorescence but weak red fluorescence, while those treated with P-α-02-B showed strong red and blue fluorescence. The results indicated that both $sC18_{4b}$ and P-α-02-B could disrupt the membranes of bacterial cells and P-α-02-B was more potent in membrane disruption than $sC18_{4b}$.

To further verify the bacterial membrane disruption caused by the peptides, the morphologies of bacterial cells were directly observed with TEM before and after being treated with $sC18_{4b}$ and P-α-02-B. As shown in Fig. 6C, the untreated *S. aureus* and *E. coli* ATCC 25922 bacterial cells, with spherical and rod-shaped morphologies respectively, presented intact and smooth cell surfaces. In contrast, obvious cell membrane damages and inner content leakages were observed in the experimental groups. The *S. aureus* and *E. coli* ATCC 25922 bacterial cells treated with $sC18_{4b}$ and P-α-02-B were out of shape, and membrane ruptures could be observed. The results indicated that P-α-02-B could kill the bacterial through disrupting their membranes.

AAMD simulation

To obtain structural insights into the interaction between P-α-02-B and the bacterial membrane, an AAMD simulation was conducted. $sC18_{4b}$ was used as a control. During the simulation, the conformations of P-α-02-B and $sC18_{4b}$ changed and reached equilibrium states as shown by the root-mean-squared distance (RMSD) (Fig. S5). During the simulation, the value of root-mean-square fluctuation (RMSF) was calculated for each residue of P-α-02-B and $sC18_{4b}$ (Fig. 7A). In general, the residues of P-α-02-B had relatively low RMSF values except those C-terminal ones. It suggested that the structure of P-α-02-B was generally rigid, except for its C-terminus, which was relatively flexible. In comparison, the structure of $sC18_{4b}$ was much looser. The secondary structure analysis validated the above findings.

As shown in Fig. 7B and C, the α-helix of $sC18_{4b}$ disintegrated and converted to a random coil at the beginning of the simulation, while P-α-02-B maintained a rigid α-helical conformation

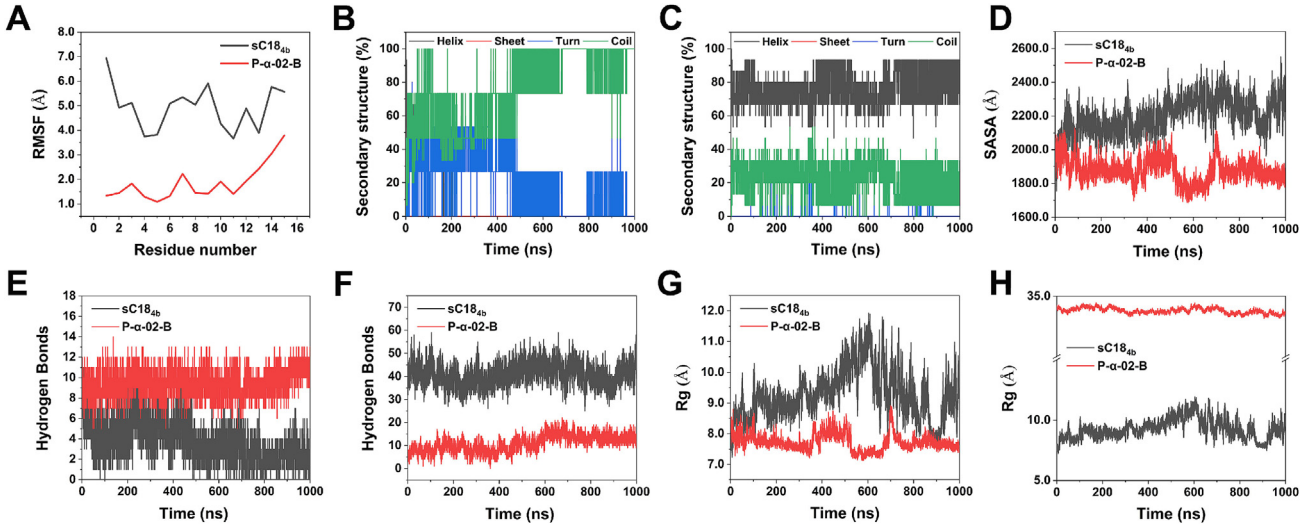

Fig. 7. Analysis on AAMD simulation of P-α-02-B and $sC18_{4b}$ interacting with phospholipid membranes. (A) RMSF calculated for each residue of P-α-02-B and $sC18_{4b}$ during the simulation; The secondary structure contents of $sC18_{4b}$ (B) and P-α-02-B (C) during the simulation; (D) The SASA calculated for $sC18_{4b}$ and P-α-02-B during the simulation; (E) The intramolecular hydrogen bonds of $sC18_{4b}$ and P-α-02-B; (F) The hydrogen bonds of $sC18_{4b}$ and P-α-02-B interacting with phospholipid membranes; (G) The Rg calculated for $sC18_{4b}$ and P-α-02-B; (H) The Rg calculated for the phospholipid membranes interacting with $sC18_{4b}$ and P-α-02-B.

throughout the whole simulation. It was critical to the bacterial membrane permeabilization. The random coil part in the secondary structure of P-α-02-B was possibly derived from its C-terminus. Interestingly, the secondary structure of $sC18_{4b}$ here was inconsistent with that measured by CD, possibly due to the discrepancy between the experimental and simulation environments. The results of solvent accessibility and hydrogen bond analysis were consistent with the above results. As shown in Fig. 7D, $sC18_{4b}$ exhibited more solvent-accessible surface area (SASA) than P-α-02-B, which could be explained by its loose random coil structure. Compared with $sC18_{4b}$, P-α-02-B had more intramolecular hydrogen bonds but fewer hydrogen bonds interacting with the phospholipid membrane, which was attributed to its rigid α-helix structure (Fig. 7E and F). The radius of gyration (Rg) can also indicate the tightness of a system. The smaller the Rg, the more compact the system is. During the simulation, P-α-02-B exhibited a smaller Rg than $sC18_{4b}$, indicating a more rigid structure. The Rg of the phospholipid membrane interacting with P-α-02-B fluctuated around 32.5 Å, approximately three times that of $sC18_{4b}$, suggesting that P-α-02-B had a stronger membrane disturbance effect than $sC18_{4b}$ (Fig. 7G and H).

Acute toxicity

To assess the acute toxicity of P-α-02-B *in vivo*, 6 Kunming mice in each group were intravenously injected with a single dose of P-α-02-B (0, 2.5, 5, 10, 15, 20, and 25 mg/kg), and the survival rate of mice was monitored within 5 days. The mice treated with P-α-02-B at doses of 0, 2.5, 5, 10 and 15 mg/kg all survived and did not show abnormal behaviors during 5 days of observation (Fig. S6). In contrast, for the groups treated with P-α-02-B at doses of 20 and 25 mg/kg, the survival rates were 33 % and 0 %, respectively. Given the above results, it was deduced that the maximal tolerated dose (MTD) is 15 mg/kg or more (but less than 20 mg/kg). Therefore, the therapeutic doses of P-α-02-B (5 and 10 mg/kg) were set lower than its MTD to guarantee safety in the following therapeutic experiments. To further explore the acute toxicity profile, the toxicity of P-α-02-B at a dose of 10 mg/kg was evaluated over an

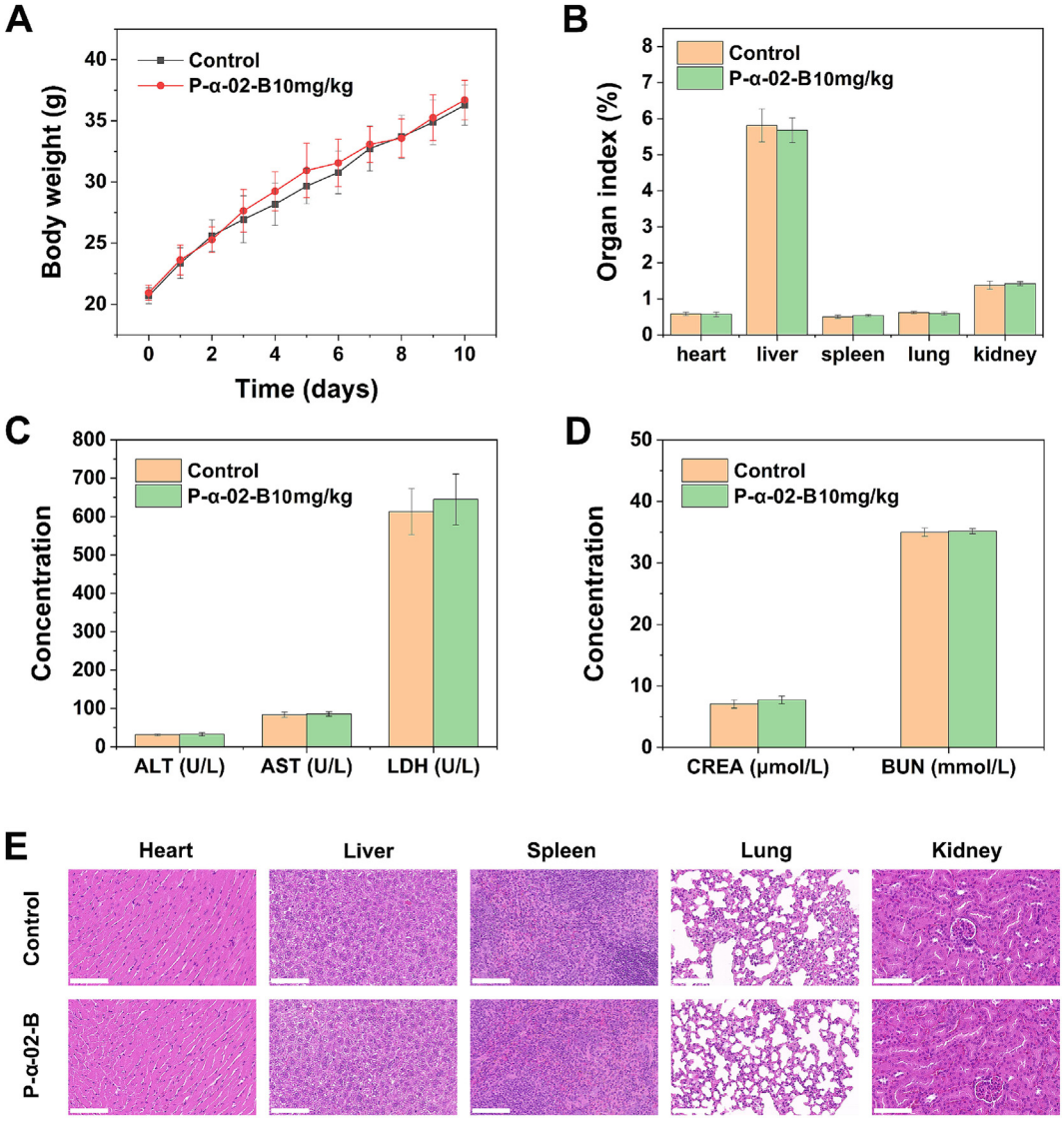

Fig. 8. *In vivo* toxicity of P-α-02-B (10 mg/kg) to mice for 10 days. (A) Weight changes of the mice after intravenous administration with a single dose of P-α-02-B (10 mg/kg); (B) Major organ indexes of the mice on day 10 after intravenous administration with a single dose of P-α-02-B (10 mg/kg); (C) Hepatic and (D) renal functional biomarkers in the blood samples collected from the mice on day 10 after intravenous administration with a single dose of P-α-02-B (10 mg/kg); The data are shown as mean ± SD (n = 5); (F) Pathological sections of organs (heart, liver, spleen, lung, kidney) stained by H&E from the mice sacrificed 10 days after being injected with P-α-02-B (10 mg/kg). The scale bar represents 0.1 mm.

extended period of 10 days. After being injected with P-α-02-B intravenously, all mice survived and did not show abnormal behaviors during 10 days of observation. The mice in the treatment group showed body weight change that was comparable to that of the control group (Fig. 8A). On day 10 post injection, the main organs and blood of mice were harvested. As shown in Fig. 8B, no significant differences were observed in the organ indexes of the main organs between the treatment group and the control group. Serum concentrations of some liver and kidney function biomarkers (Fig. 8C and D), including alanine aminotransferase (ALT), aspartate aminotransferase (AST), lactate dehydrogenase (LDH), creatinine (CREA) and blood urea nitrogen (BUN), as well as some hematological parameters (Table S3), including counts of WBC, red blood cell (RBC), hemoglobin (HGB), platelet (PLT), neutrophils (NEUT) and lymphocyte (LYMPH), were tested. The above parameters were not significantly different between the two groups, indicating that the P-α-02-B administration had no adverse effect on the hepatic, renal functions and hematological parameters of mice. Compared with the control group, no obvious histopathological changes were observed in the treatment group (Fig. 8E). Taken together, these results suggested that intravenous administration of P-α-02-B at a therapeutic dose of ≤ 10 mg/kg was safe in mice.

In vivo antimicrobial activity

P-α-02-B was proven to have potent antimicrobial activity *in vitro*, whether used alone or in combination with levofloxacin, and then its antimicrobial efficacy *in vivo* was also investigated by an *S. aureus*-infected mouse model. The mice were divided into a control group (uninfected), a saline group, and five administration groups including low P-α-02-B group (5 mg/kg); high P-α-02-B group (10 mg/kg); levofloxacin group (2.5 mg/kg); levofloxacin + low P-α-02-B group (2.5 mg/kg + 5 mg/kg); levofloxacin + high P-α-02-B group (2.5 mg/kg + 10 mg/kg). The mice were administrated with fixed dosage twice a day (Fig. 9A). The mice of the control group kept alive for 3 days, while the bacterial infected mice started to die on day 1, with three-day survival rate of 25 %∼87.5 % (Fig. 9B). Five administration groups demonstrated obvious therapeutic effects, as their survival rates were

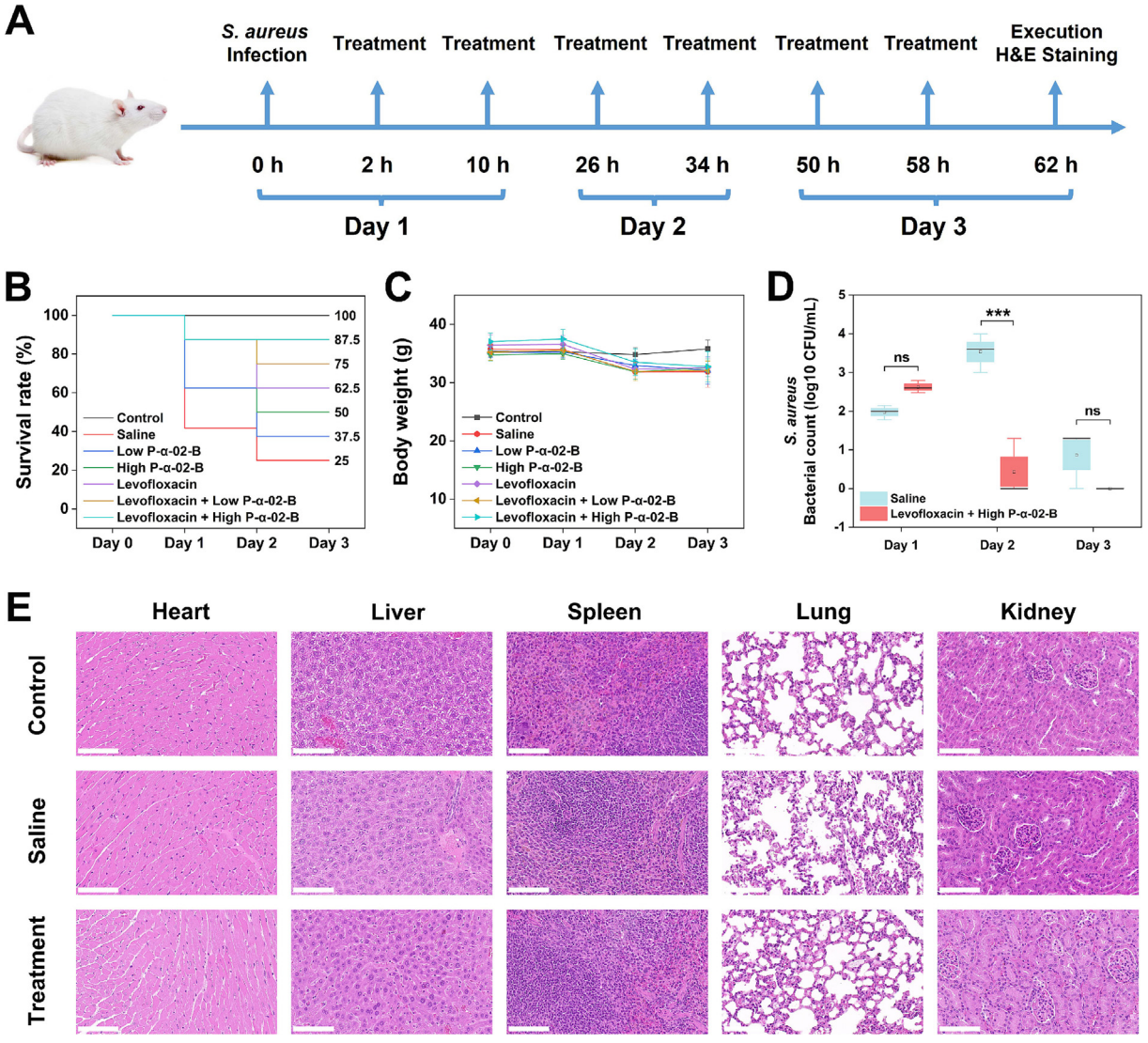

Fig. 9. In vivo efficacy of P-α-02-B alone or in combination with levofloxacin using an *S. aureus*-infected mouse model. (A) Experimental workflow of the therapeutic process; Survival cure (B) and average body weight (C) of mice treated with saline and different antimicrobial agents. The mice in the control group were not inoculated with bacteria; (D) Blood bacterial count of mice treated with saline and P-α-02-B (10 mg/kg) in combination with levofloxacin (2.5 mg/kg). ***$P < 0.001$, ns: no significance; (E) Pathological sections of mouse organs (heart, liver, spleen, lung, kidney) stained by H&E. The scale bar represents 0.1 mm.

observed to be higher than that of the saline group. P-α-02-B showed stronger therapeutic effects at high dose (10 mg/kg) than at low dose (5 mg/kg), whether administered alone or in combination with levofloxacin, which agreed with the above results. Notably, the mice treated with P-α-02-B in combination with levofloxacin showed higher survival rates than those treated with each drug alone at the same doses, indicating the synergistic effect *in vivo*. Taken together, P-α-02-B (10 mg/kg) in combination with levofloxacin (2.5 mg/kg) demonstrated the strongest therapeutic effect *in vivo*.

The body weights of mice were kept track of throughout the entire experiment. The average body weight of the mice in the control group barely changed (Fig. 9C). In contrast, a slightly body weight loss was observed for all the *S. aureus*-infected mice. The bacterial count in the blood of mice treated with saline and P-α-02-B (10 mg/kg) in combination with levofloxacin (2.5 mg/kg) was shown in Fig. 9D. Compared with the saline group, the administration group showed a greater reduction in the bacterial load in blood. As shown in Fig. 9E, H&E staining was performed to examine the histopathological changes in several organs of mice. In the saline group, obvious histopathological changes were observed in the liver and lung tissues, including inflammatory cell infiltration and alveolar hemorrhage. There were no obvious histopathological changes in the heart, spleen, and kidney tissues. Notably, the treatment of P-α-02-B (10 mg/kg) in combination with levofloxacin (2.5 mg/kg) significantly alleviated inflammation and hemorrhage reactions, when compared to the saline group. Taken together, P-α-02-B, whether used alone or in combination with levofloxacin, could effectively suppress bacterial infection *in vivo*.

The PK study in vivo

For most AMPs, the antimicrobial activity can be greatly influenced by their absorption, distribution, metabolism, and excretion in the body. Therefore, the PK properties of P-α-02-B were further studied. As shown in Fig. S7A, the P-α-02-B administered intravenously at a dose of 5 mg/kg was initially detected at a plasma concentration of 24723.09n g/mL 2 min post-administration and declined to its lowest level 4 h post-administration. The half-life calculated for P-α-02-B was 0.66 h (Fig. S7B), exceeding that (0.39 h) of the commercially available antimicrobial peptide drug polymyxin E [52]. It indicated that P-α-02-B showed great potential in the development of antimicrobial therapeutics.

Declaration of competing interest

The authors declare that they have no known competing financial interests or personal relationships that could have appeared to influence the work reported in this paper.

Acknowledgements

This study was supported by National Natural Science Foundation of China (No. 22171286, China).

Appendix A. Supplementary data

Supplementary data to this article can be found online at https://doi.org/10.1016/j.jare.2025.01.029.

References

[1] De Oliveira DMP, Forde BM, Kidd TJ, Harris PNA, Schembri MA, Beatson SA, et al. Antimicrobial resistance in ESKAPE pathogens. Clin Microbiol Rev 2020;33:e00181–219. doi: https://doi.org/10.1128/CMR.00181-19.

[2] Peyrani P, Mandell L, Torres A, Tillotson GS. The burden of community-acquired bacterial pneumonia in the era of antibiotic resistance. Expert Rev Respir Med 2019;13:139–52. doi: https://doi.org/10.1080/17476348.2019.1562339.

[3] Rawson TM, Moore LSP, Zhu N, Ranganathan N, Skolimowska K, Gilchrist M, et al. Bacterial and fungal coinfection in individuals with coronavirus: a rapid review to support COVID-19 antimicrobial prescribing. Clin Infect Dis 2020;71:2459–68. doi: https://doi.org/10.1093/cid/ciaa530.

[4] Magana M, Pushpanathan M, Santos AL, Leanse L, Fernandez M, Ioannidis A, et al. The value of antimicrobial peptides in the age of resistance. Lancet Infect Dis 2020;20:e216–30. doi: https://doi.org/10.1016/S1473-3099(20)30327-3.

[5] Kumar P, Kizhakkedathu J, Straus S. Antimicrobial peptides: diversity, mechanism of action and strategies to improve the activity and biocompatibility in vivo. Biomolecules 2018;8:4. doi: https://doi.org/10.3390/biom8010004.

[6] Browne K, Chakraborty S, Chen R, Willcox MD, Black DS, Walsh WR, et al. A new era of antibiotics: the clinical potential of antimicrobial peptides. Int J Mol Sci 2020;21:7047. doi: https://doi.org/10.3390/ijms21197047.

[7] Mahlapuu M, Håkansson J, Ringstad L, Björn C. Antimicrobial peptides: an emerging category of therapeutic agents. Front Cell Infect Microbiol 2016;6:194. doi: https://doi.org/10.3389/fcimb.2016.00194.

[8] Mwangi J, Hao X, Lai R, Zhang ZY. Antimicrobial peptides: new hope in the war against multidrug resistance. Zool Res 2019;40:488–505. doi: https://doi.org/10.24272/j.issn.2095-8137.2019.062.

[9] Zasloff M. Antimicrobial peptides of multicellular organisms. Nature 2002;415:389–95. doi: https://doi.org/10.1038/415389a.

[10] Zhong C, Zhang F, Zhu N, Zhu Y, Yao J, Gou S, et al. Ultra-short lipopeptides against gram-positive bacteria while alleviating antimicrobial resistance. Eur J Med Chem 2021;212:. doi: https://doi.org/10.1016/j.ejmech.2020.113138113138.

[11] Zhu N, Zhong C, Liu T, Zhu Y, Gou S, Bao H, et al. Newly designed antimicrobial peptides with potent bioactivity and enhanced cell selectivity prevent and reverse rifampin resistance in gram-negative bacteria. Eur J Pharm Sci 2021;158:. doi: https://doi.org/10.1016/j.ejps.2020.105665105665.

[12] Jayathilaka EHTT, Rajapaksha DC, Nikapitiya C, De Zoysa M, Whang I. Antimicrobial and anti-biofilm peptide octominin for controlling multidrug-resistant Acinetobacter baumannii. Int J Mol Sci 2021;22:5353. doi: https://doi.org/10.3390/ijms22105353.

[13] Peng J, Mishra B, Khader R, Felix L, Mylonakis E. Novel Cecropin-4 derived peptides against methicillin-resistant Staphylococcus aureus. Antibiotics 2021;10:36. doi: https://doi.org/10.3390/antibiotics10010036.

[14] Dijksteel GS, Ulrich MMW, Middelkoop E, Boekema BKHL. Review: Lessons Learned From Clinical Trials Using Antimicrobial Peptides (AMPs). Front Microbiol 2021;12:. doi: https://doi.org/10.3389/fmicb.2021.616979616979.

[15] Bobone S, Stella L. Selectivity of antimicrobial peptides: a complex interplay of multiple equilibria. Advances in Experimental Medicine and Biology 2019;1117:175–214. doi: https://doi.org/10.1007/978-981-13-3588-4_11.

[16] Chen Y, Guarnieri MT, Vasil AI, Vasil ML, Mant CT, Hodges RS. Role of peptide hydrophobicity in the mechanism of action of α-helical antimicrobial peptides. Antimicrob Agents Chemother 2007;51:1398–406. doi: https://doi.org/10.1128/AAC.00925-06.

[17] Duque HM, Rodrigues G, Santos LS, Franco OL. The biological role of charge distribution in linear antimicrobial peptides. Expert Opin Drug Discov 2023;18:287–302. doi: https://doi.org/10.1080/17460441.2023.2173736.

[18] Torres MDT, Sothiselvam S, Lu TK, De La Fuente-Nunez C. Peptide design principles for antimicrobial applications. J Mol Biol 2019;431:3547–67. doi: https://doi.org/10.1016/j.jmb.2018.12.015.

[19] Lai Z, Yuan X, Chen H, Zhu Y, Dong N, Shan A. Strategies employed in the design of antimicrobial peptides with enhanced proteolytic stability. Biotechnol Adv 2022;59:. doi: https://doi.org/10.1016/j.biotechadv.2022.107962107962.

[20] Lu J, Xu H, Xia J, Ma J, Xu J, Li Y, et al. D- and unnatural amino acid substituted antimicrobial peptides with improved proteolytic resistance and their proteolytic degradation characteristics. Front Microbiol 2020;11:. doi: https://doi.org/10.3389/fmicb.2020.563030563030.

[21] Sandín D, Valle J, Chaves-Arquero B, Prats-Ejarque G, Larrosa MN, González-López JJ, et al. Rationally modified antimicrobial peptides from the N-terminal domain of human RNase 3 show exceptional serum stability. J Med Chem 2021;64:11472–82. doi: https://doi.org/10.1021/acs.jmedchem.1c00795.

[22] Wade D, Boman A, Wåhlin B, Drain CM, Andreu D, Boman HG, et al. All-D amino acid-containing channel-forming antibiotic peptides. Proc Natl Acad Sci 1990;87:4761–5. doi: https://doi.org/10.1073/pnas.87.12.4761.

[23] Oo TZ, Cole N, Garthwaite L, Willcox MDP, Zhu H. Evaluation of synergistic activity of bovine lactoferricin with antibiotics in corneal infection. J Antimicrob Chemother 2010;65:1243–51. doi: https://doi.org/10.1093/jac/dkq106.

[24] Krieger E, Vriend G. YASARA View—molecular graphics for all devices—from smartphones to workstations. Bioinformatics 2014;30:2981–2. doi: https://doi.org/10.1093/bioinformatics/btu426.

[25] Krieger E, Dunbrack RL, Hooft RWW, Krieger B. Assignment of protonation states in proteins and ligands: combining pKa prediction with hydrogen bonding network optimization. Methods Mol Biol 2012;819:405–21. doi: https://doi.org/10.1007/978-1-61779-465-0_25.

[26] Krieger E, Nielsen JE, Spronk CAEM, Vriend G. Fast empirical pKa prediction by Ewald summation. J Mol Graph Model 2006;25:481–6. doi: https://doi.org/10.1016/j.jmgm.2006.02.009.

[27] Essmann U, Perera L, Berkowitz ML, Darden T, Lee H, Pedersen LG. A smooth particle mesh Ewald method. J Chem Phys 1995;103:8577–93. doi: https://doi.org/10.1063/1.470117.
[28] Krieger E, Vriend G. New ways to boost molecular dynamics simulations. J Comput Chem 2015;36:996–1007. doi: https://doi.org/10.1002/jcc.23899.
[29] Drexelius M, Reinhardt A, Grabeck J, Cronenberg T, Nitsche F, Huesgen PF, et al. Multistep optimization of a cell-penetrating peptide towards its antimicrobial activity. Biochem J 2021;478:63–78. doi: https://doi.org/10.1042/BCJ20200698.
[30] Bellavita R, Braccia S, Galdiero S, Falanga A. Glycosylation and Lipidation Strategies: Approaches for Improving Antimicrobial Peptide Efficacy. Pharmaceuticals 2023;16:439. doi: https://doi.org/10.3390/ph16030439.
[31] Koh JJ, Lin H, Caroline V, Chew YS, Pang LM, Aung TT, et al. N-Lipidated Peptide Dimers: Effective Antibacterial Agents against Gram-Negative Pathogens through Lipopolysaccharide Permeabilization. J Med Chem 2015;58:6533–48. doi: https://doi.org/10.1021/acs.jmedchem.5b00628.
[32] Liu Y, Shen T, Chen L, Zhou J, Wang C. Analogs of the Cathelicidin-Derived Antimicrobial Peptide PMAP-23 Exhibit Improved Stability and Antibacterial Activity, Probiotics Antimicrob. Proteins 2021;13:273–86. doi: https://doi.org/10.1007/s12602-020-09686-z.
[33] Mishra B, Felix L, Basu A, Kollala SS, Chhonker YS, Ganesan N, et al. Design and Evaluation of Short Bovine Lactoferrin-Derived Antimicrobial Peptides against Multidrug-Resistant Enterococcus faecium. Antibiotics 2022;11:1085. doi: https://doi.org/10.3390/antibiotics11081085.
[34] Mishra B, Reiling S, Zarena D, Wang G. Host defense antimicrobial peptides as antibiotics: design and application strategies. Curr Opin Chem Biol 2017;38:87–96. doi: https://doi.org/10.1016/j.cbpa.2017.03.014.
[35] Ciumac D, Gong H, Hu X, Lu JR. Membrane targeting cationic antimicrobial peptides. J Colloid Interface Sci 2019;537:163–85. doi: https://doi.org/10.1016/j.jcis.2018.10.103.
[36] Preußke N, Lipfert M, Rothemund S, Leippe M, Sönnichsen FD. Designed Trp-Cage Proteins with Antimicrobial Activity and Enhanced Stability. Biochemistry 2021;60:3187–99. doi: https://doi.org/10.1021/acs.biochem.1c00567.
[37] Wolny M, Batchelor M, Bartlett GJ, Baker EG, Kurzawa M, Knight PJ, et al. Characterization of long and stable de novo single alpha-helix domains provides novel insight into their stability. Sci Rep 2017;7(2017):44341. doi: https://doi.org/10.1038/srep44341.
[38] Jiang Z, Vasil AI, Hale JD, Hancock REW, Vasil ML, Hodges RS. Effects of net charge and the number of positively charged residues on the biological activity of amphipathic α-helical cationic antimicrobial peptides. Pept Sci 2008;90:369–83. doi: https://doi.org/10.1007/978-0-387-73657-0_246.
[39] Chen C, Yang C, Chen Y, Wang F, Mu Q, Zhang J, et al. Surface Physical Activity and Hydrophobicity of Designed Helical Peptide Amphiphiles Control Their Bioactivity and Cell Selectivity. ACS Appl Mater Interfaces 2016;8:26501–10. doi: https://doi.org/10.1021/acsami.6b08297.
[40] Edwards IA, Elliott AG, Kavanagh AM, Zuegg J, Blaskovich MAT, Cooper MA. Contribution of Amphipathicity and Hydrophobicity to the Antimicrobial Activity and Cytotoxicity of β-Hairpin Peptides. ACS Infect Dis 2016;2:442–50. doi: https://doi.org/10.1021/acsinfecdis.6b00045.
[41] Gupta K, Singh S, Van Hoek M. Short, Synthetic Cationic Peptides Have Antibacterial Activity against Mycobacterium smegmatis by Forming Pores in Membrane and Synergizing with Antibiotics. Antibiotics 2015;4:358–78. doi: https://doi.org/10.3390/antibiotics4030358.
[42] Lewies A, Wentzel JF, Jordaan A, Bezuidenhout C, Du Plessis LH. Interactions of the antimicrobial peptide nisin Z with conventional antibiotics and the use of nanostructured lipid carriers to enhance antimicrobial activity. Int J Pharm 2017;526:244–53. doi: https://doi.org/10.1016/j.ijpharm.2017.04.071.
[43] Zharkova MS, Orlov DS, Golubeva OY, Chakchir OB, Eliseev IE, Grinchuk TM, et al. Application of Antimicrobial Peptides of the Innate Immune System in Combination With Conventional Antibiotics—A Novel Way to Combat Antibiotic Resistance? Front Cell Infect Microbiol 2019;9:128. doi: https://doi.org/10.3389/fcimb.2019.00128.
[44] Bush NG, Diez-Santos I, Abbott LR, Maxwell A. Quinolones: Mechanism, Lethality and Their Contributions to Antibiotic Resistance. Molecules 2020;25:5662. doi: https://doi.org/10.3390/molecules25235662.
[45] Akbari R, Hakemi-Vala M, Pashaie F, Bevalian P, Hashemi A, Pooshang Bagheri K. Highly Synergistic Effects of Melittin with Conventional Antibiotics Against Multidrug-Resistant Isolates of Acinetobacter baumannii and Pseudomonas aeruginosa. Microb Drug Resist 2019;25:193–202. doi: https://doi.org/10.1089/mdr.2018.0016.
[46] Chatupheeraphat C, Peamchai JJ, Luk-in S, Eiamphungporn W. Synergistic effect and antibiofilm activity of the antimicrobial peptide K11 with conventional antibiotics against multidrug-resistant and extensively drug-resistant Klebsiella pneumoniae. Front Cell Infect Microbiol 2023;13:. doi: https://doi.org/10.3389/fcimb.2023.1153868 1153868.
[47] Jahangiri A, Neshani A, Mirhosseini SA, Ghazvini K, Zare H, Sedighian H. Synergistic effect of two antimicrobial peptides, Nisin and P10 with conventional antibiotics against extensively drug-resistant Acinetobacter baumannii and colistin-resistant Pseudomonas aeruginosa isolates. Microb Pathog 2021;150:. doi: https://doi.org/10.1016/j.micpath.2020.104700 104700.
[48] Di YP, Lin Q, Chen C, Montelaro RC, Doi Y, Deslouches B. Enhanced therapeutic index of an antimicrobial peptide in mice by increasing safety and activity against multidrug-resistant bacteria. Sci Adv 2020;6(18):. doi: https://doi.org/10.1126/sciadv.aay6817 eaay6817.
[49] Kim H, Jang JH, Kim SC, Cho JH. Development of a novel hybrid antimicrobial peptide for targeted killing of Pseudomonas aeruginosa. Eur J Med Chem 2020;185:. doi: https://doi.org/10.1016/j.ejmech.2019.111814 111814.
[50] Lehrer RI, Barton A, Daher KA, Harwig SS, Ganz T, Selsted ME. Interaction of human defensins with Escherichia coli. Mechanism of bactericidal activity. J Clin Invest 1989;84:553–61. doi: https://doi.org/10.1172/JCI114198.
[51] Turner J, Cho Y, Dinh NN, Waring AJ, Lehrer RI. Activities of LL-37, a Cathelin-Associated Antimicrobial Peptide of Human Neutrophils. Antimicrob Agents Chemother 1998;42:2206–14. doi: https://doi.org/10.1128/AAC.42.9.2206.
[52] Li J, Milne RW, Nation RL, Turnidge JD, Smeaton TC, Coulthard K. Pharmacokinetics of colistin methanesulphonate and colistin in rats following an intravenous dose of colistin methanesulphonate. J Antimicrob Chemother 2004;53:837–40. doi: https://doi.org/10.1093/jac/dkh167.